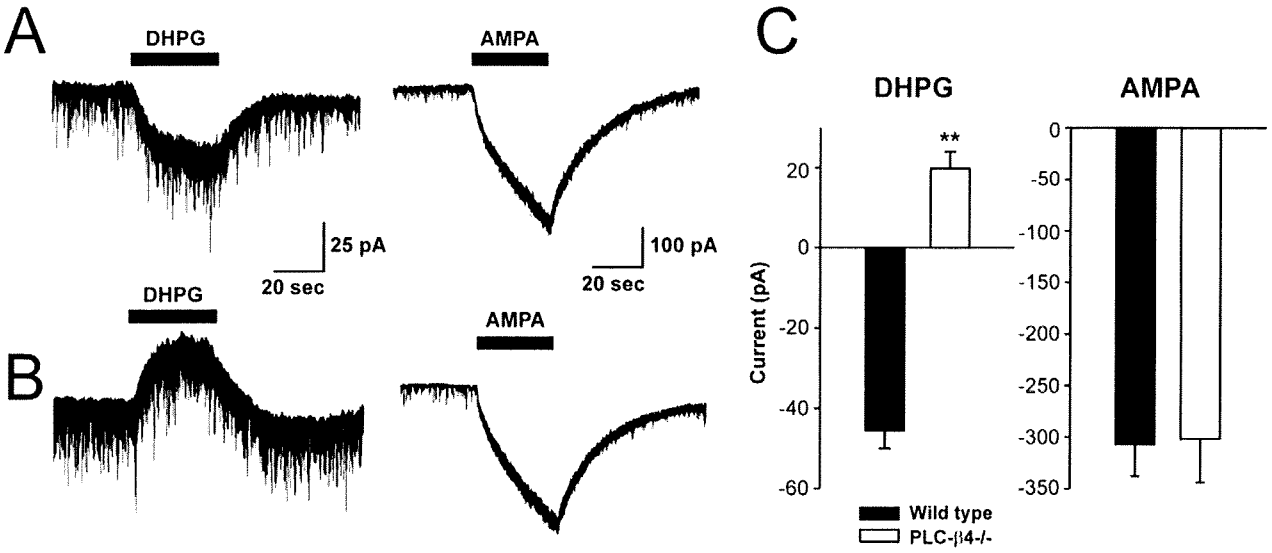

Figure 5. Responses of LGNd relay neurons to DHPG were examined using whole-cell voltage-clamp recordings. DHPG (200 μM) induced inward currents in LGNd relay-neurons in wild-type mice (**A**) but produced outward currents at the same holding membrane potential (−70 mV) in PLC-β4−/− mice (**B**). Stimulation of the same neurons with AMPA (10 μM) induced large inward currents in both wild-type (**A**) and PLC-β4−/− mice (**B**). **C.** The mean current amplitude was calculated and compared (error bars denote S.E.M.) n = 13–15 for each group. $^{**}P<0.01$ compared with the wild-type group by Student's *t*-test. All experiments were conducted in the presence of 1 μM tetrodotoxin.
doi:10.1371/journal.pone.0007737.g005

between orexin receptors and PLC-β4 in the LGNd, neuronal network communications among the LGNd, the rostral-midline thalamus, and/or other orexin-positive nuclei thus appear to have a role in regulation of sleep stages and sequences.

In conclusion, the present results demonstrate that PLC-β4−/− mice display fragmented sleep with unusual wake-to-REM sleep transitions, both during the day and nighttime. Also, PLC-β4−/− mice reduced ultradian body temperature rhythms and elevated body temperatures during the daytime. Although critical site(s) of PLC-β4−/− actions to produce these behavioral phenotypes are still remaining to be determined, localized expression of PLC-β4 in the brain lead us to propose that the most likely site is the LGNd. In fact, we demonstrated disrupted group-1 mGluR signaling in LGNd relay neurons in the PLC-β4−/− mice. Thus, the present results support the suggested thalamic function for the transition and maintenance of sleep stages.

Acknowledgments

The authors would like to thank Yuko Kuwahata for excellent sleep EEG recordings and Dr. Osamu Hayaishi (Osaka Bioscience Institute) for helpful comments on this project.

Author Contributions

Conceived and designed the experiments: MI NE YU TY. Performed the experiments: MI MH TS TM. Analyzed the data: MI MIS NE TY. Contributed reagents/materials/analysis tools: TS YU TY. Wrote the paper: MI.

References

1. Jones BE (1991) Paradoxical sleep and its chemical/structural substrates in the brain. Neuroscience 40: 637–656.
2. McCarley RW (1999) Sleep neurophysiology: Basic mechanisms underlying control of wakefulness and sleep. In: Chokroverty S, ed. Sleep Disorders Medicine: Basic Science, Technical Considerations, and Clinical Aspects. Boston: Butterworth Heinemann. pp 21–50.
3. Lin L, Faraco J, Li R, Kadotani H, Rogers W, et al. (1999) The sleep disorder canine narcolepsy is caused by a mutation in the hypocretin (orexin) receptor 2 gene. Cell 98: 365–376.
4. Chemelli RM, Willie JT, Sinton CM, Elmquist JK, Scammell T, et al. (1999) Narcolepsy in orexin knockout mice: molecular genetics of sleep regulation. Cell 98: 437–451.
5. Mochizuki T, Crocker A, McCormack S, Yanagisawa M, Sakurai T, et al. (2004) Behavioral state instability in orexin knock-out mice. J Neurosci 24: 6291–6300.
6. Zhang S, Zeitzer JM, Sakurai T, Nishino S, Mignot E (2007) Sleep/wake fragmentation disrupts metabolism in a mouse model of narcolepsy. J Physiol 581: 649–663.
7. Thakker MM, Ramesh V, Cape EG, Winston S, Strecker RE, et al. (1999) REM sleep enhancement and behavioral cataplexy following orexin (hypocretin)-II receptor antisense perfusion in the pontine reticular formation. Sleep Res Online 2: 112–120.
8. Hagan JJ, Leslie RA, Patel S, Evans ML, Wattam TA, et al. (1999) Orexin A activates locus coeruleus cell firing and increases arousal in the rat. Proc Natl Acad Sci U S A 96: 10911–10916.
9. Bayer L, Eggermann E, Saint-Mleux B, Machard D, Jones BE, et al. (2002) Selective action of orexin (hypocretin) on nonspecific thalamocortical projection neurons. J Neurosci 22: 7835–7839.
10. Govindaiah G, Cox CL (2006) Modulation of thalamic neuron excitability by orexins. Neuropharmacology 51: 414–425.
11. Peyron C, Tighe DK, van den Pol AN, de Lecea L, Heller HC, et al. (1998) Neurons containing hypocretin (orexin) project to multiple neuronal systems. J Neurosci 18: 9996–10015.
12. Sakurai T, Amemiya A, Ishii M, Matsuzaki I, Chemelli RM, et al. (1998) Orexin and orexin receptors: a family of hypothalamic neuropeptides and G-protein-coupled receptors that regulate feeding behavior. Cell 92: 573–585.
13. Sugiyama T, Hirono M, Suzuki K, Nakamura Y, Aiba A, et al. (1999) Localization of phospholipase Cbeta isozymes in the mouse cerebellum. Biochem Biophy Res Commun 265: 473–478.
14. Hirono M, Sugiyama T, Kishimoto Y, Sakai I, Miyazawa T, et al. (2001) Phospholipase Cβ4 and protein kinase Cα and/or protein kinase CβI are involved in the induction of long term depression in cerebellar Purkinje cells. J Biol Chem 276: 45236–45242.
15. Jiang H, Lyubarsky A, Dodd R, Vardi N, Pugh E, et al. (1996) Phospholipase C beta 4 is involved in modulating the visual response in mice. Proc Natl Acad Sci USA 93: 14598–1460.
16. Kameyama M, Yamaguchi I, Ichikawa K, Sugiyama T, Hirono M, et al. (2003) Effect of phospholipase Cβ4 lacking in thalamic neurons on electroencephalogram. Biochem Biophys Res Commun 304: 153–159.
17. McCormick DA, von Krosigk M (1992) Corticothalamic activation modulates thalamic firing through glutamate "metabotropic" receptors. Proc Natl Acad Sci USA 89: 2774–2778.
18. Lee KH, McCormick DA (1997) Modulation of spindle oscillations by acetylcholine, cholecystokinin and 1S,3R-ACPD in the ferret lateral geniculate and perigeniculate nuclei in vitro. Neuroscience 77: 335–350.

19. Steriade M (2000) Corticothalamic resonance states of vigilance and mentation. Neuroscience 101: 243–276.
20. Pinzar E, Kanaoka Y, Inui T, Eguchi N, Urade Y, et al. (2000) Prostaglandin D synthase gene is involved in the regulation of non-rapid eye movement sleep. Proc Natl Acad Sci U S A 97: 4903–4907.
21. Tobler I, Deboer T, Fischer M (1997) Sleep and sleep regulation in normal and prion protein-deficient mice. J Neurosci 17: 1869–1879.
22. Ikeda M, Sugiyama T, Suzuki T, Moriya T, Shibata S, et al. (2000a) PLC β4-independent Ca^{2+} rise via muscarinic receptors in the mouse suprachiasmatic nucleus. Neuroreport 11: 907–912.
23. Godwin DW, Vaughan JW, Sherman SM (1996) Metabotropic glutamate receptors switch visual response mode of lateral geniculate nucleus cells from burst to tonic. J Neurophysiol 76: 1800–1816.
24. Cox CL, Zhou QZ, Sherman SM (1998) Glutamate locally activates dendritic outputs of thalamic interneurons. Nature 394: 478–482.
25. Miller AM, Obermeyer WH, Behan M, Benca RM (1998) The superior colliculus-pretectum mediates the direct effects of light on sleep. Proc Natl Acad Sci USA 95: 8957–8962.
26. Miller AM, Miller RB, Obermeyer WH, Behan M, Benca RM (1999) The pretectum mediates rapid eye movement sleep regulation by light. Behav Neurosci 113: 755–765.
27. Ikeda M, Sagara M, Inoué S (2000b) Continuous exposure to dim illumination uncouples temporal patterns of sleep, body temperature, locomotion and drinking behavior in the rat. Neurosci Lett 279: 185–189.
28. Jenkins TC, Andrews JB, Meyer-Bernstein EL (2007) Daily oscillation of phospholipase C β4 in the mouse suprachiasmatic nucleus. Brain Res 1178: 83–91.
29. Wurts SW, Edgar DM (2000) Circadian and homeostatic control of rapid eye movement (REM) sleep: promotion of REM tendency by the suprachiasmatic nucleus. J Neurosci 20: 4300–4310.
30. Deboer T, Vansteensel MJ, Détári L, Meijer JH (2003) Sleep states alter activity of suprachiasmatic nucleus neurons. Nat Neurosci 6: 1086–1090.
31. Vidnyánszky Z, Gorcs TJ, Negyessy L, Borostyankio Z, Knopfel T, et al. (1996) Immunocytochemical visualization of the mGluR1a metabotropic glutamate receptor at synapses of corticothalamic terminals originating from area 17 of the rat. Eur J Neurosci 8: 1061–1071.
32. Lourenco Neto F, Schadrack J, Berthele A, Zieglgänsberger W, Tölle TR, et al. (2000) Differential distribution of metabotropic glutamate receptor subtype mRNAs in the thalamus of the rat. Brain Res 854: 93–105.
33. Kim D, Jun KS, Lee SB, Kang NG, Min DS, et al. (1997) Phospholipase C isozymes selectively couple to specific neurotransmitter receptors. Nature 389: 290–293.
34. White AM, Kylänpää RA, Christie LA, McIntosh SJ, Irving AJ, et al. (2003) Presynaptic group I metabotropic glutamate receptors modulate synaptic transmission in the rat superior colliculus via 4-AP sensitive K^+ channels. Br J Pharmacol 140: 1421–1433.
35. Boutrel B, Franc B, Hen R, Hamon M, Adrien J (1999) Key role of 5-HT1B receptors in the regulation of paradoxical sleep as evidenced in 5-HT1B knock-out mice. J Neurosci 19: 3204–3212.
36. Hunsley MS, Curtis WR, Palmiter RD (2006) Behavioral and sleep/wake characteristics of mice lacking norepinephrine and hypocretin. Genes Brain Behav 5: 451–457.
37. Hunsley MS, Palmiter RD (2003) Norepinephrine-deficient mice exhibit normal sleep-wake states but have shorter sleep latency after mild stress and low doses of amphetamine. Sleep 26: 521–526.
38. Parmentier R, Ohtsu H, Djebbara-Hannas Z, Valatx JL, Watanabe T, et al. (2002) Anatomical, physiological, and pharmacological characteristics of histidine decarboxylase knock-out mice: Evidence for the role of brain histamine in behavioral and sleep-wake control. J Neurosci 22: 7695–7711.
39. Anderson MP, Mochizuki T, Xie J, Fischler W, Manger JP, et al. (2005) Thalamic $Ca_v3.1$ T-type Ca^{2+} channel plays a crucial role in stabilizing sleep. Proc Natl Acad Sci USA 102: 1743–1748.

Neuroscience 155 (2008) 454–462

INVOLVEMENT OF CYCLOOXYGENASE-2 IN LIPOPOLYSACCHARIDE-INDUCED IMPAIRMENT OF THE NEWBORN CELL SURVIVAL IN THE ADULT MOUSE DENTATE GYRUS

G. N. BASTOS,[a] T. MORIYA,[a]* F. INUI,[a] T. KATURA[a] AND N. NAKAHATA[a,b]

[a]*Department of Cellular Signaling, Graduate School of Pharmaceutical Sciences, Tohoku University, Aramaki, Aoba-ku, Sendai 980-8578, Japan*

[b]*21st Century COE program "CRESCENDO," Graduate School of Pharmaceutical Sciences, Tohoku University, Sendai 980-8578, Japan*

Abstract—There is growing evidence indicating that neurogenesis in adulthood is influenced by certain types of the central diseases such as neuroinflammation, however, its mechanism is not fully understood. This study was, therefore, designed to examine the effects of lipopolysaccharide (LPS), a bacterial endotoxin known to cause the neuroinflammation, on the neurogenesis in the dentate gyrus of adult mice using the bromodeoxyuridine (BrdU) –pulse chase method. LPS failed to affect the number of BrdU-labeled cells in the dentate gyrus 2 h after BrdU injection, indicating no effects of LPS on the proliferation of the neural stem cells (NSCs). On the other hand, we found that LPS dose-dependently (0.1, 0.5, 1 mg/kg) decreased the number of BrdU-labeled cells 7 and 21 days after BrdU injection. We also observed that LPS increased cell death in the dentate gyrus using terminal deoxynucleotidyl transferase-mediated dUTP nick end-labeling (TUNEL) staining, suggesting that LPS impaired the survival of newborn cells derived from the NSCs. The double-immunostaining for BrdU and specific cell type markers revealed that LPS did not alter the commitment of the NSCs to the neurons and astrocytes. The systemic injection of indomethacin, a non-selective cyclooxygenase (COX) inhibitor, and NS398, a selective COX-2 inhibitor, but not SC560, a selective COX-1 inhibitor, did not only ameliorate LPS-induced suppression of the newborn cell survival, they fully protected against the LPS effect. Furthermore, the central injection of NS398 also ameliorated LPS-induced suppression of the newborn cell survival in the dentate gyrus. The treatment with LPS increased the expression of COX-2 protein 7 h and 7 days after the injection in the dentate gyrus. These results suggest that LPS impairs the survival of newly generated cells derived from the NSCs in the dentate gyrus without affecting the differentiation fate, and these effects of LPS were mediated presumably by COX-2 expression in the dentate gyrus.

Key words: dentate gyrus, lipopolysaccharide, neural stem cells, survival, bromodeoxyuridine.

*Corresponding author. Tel: +81-22-795-3843; fax: +81-22-795-3847.
E-mail address: moriya@mail.pharm.tohoku.ac.jp (T. Moriya).

Abbreviations: BrdU, bromodeoxyuridine; COX, cyclooxygenase; DCX, doublecortin; GCL, granule cell layer; GFAP, glial fibrillary acidic protein; LPS, lipopolysaccharide; ML, molecular layer; NeuN, neuronal nuclei protein; NSCs, neural stem cells; PB, phosphate buffer; PBS, phosphate-buffered saline; PBSGT, phosphate-buffered saline containing 1% normal goat serum and 0.3% Triton X-100; PGD_2, prostaglandin D_2; PGE_2, prostaglandin E_2; TUNEL, terminal deoxynucleotidyl transferase-mediated dUTP nick end-labeling; 15d-PGJ_2, 15-deoxy-prostaglandin J_2.

Recent studies have revealed that the neural stem cells (NSCs), which possess the ability of proliferation and differentiation into neurons and glial cells (Ono et al., 2001), exist in the mammalian adult brain, including the anterior subventricular zone (aSVZ) and the hippocampal dentate gyrus (Gage, 2002). The NSCs in the dentate gyrus are known to lie along the border between the hilus and the granule cell layer (GCL), so called subgranular zone (SGZ), and to migrate into the GCL and to differentiate into the glial cells and the granule cells, resulting in the generation of several thousands of newborn cells each day (Cameron and McKay, 2001; Christie and Cameron, 2006). Furthermore, the small portion of newly generated neurons is reported to be integrated into existing neuronal circuitries (Mandyam et al., 2007). The role of neurogenesis in the dentate gyrus is still unclear, however, several lines of evidence suggest its involvement in the learning and memory (Gould et al., 1999, 2000; Shors et al., 2001; Aimone et al., 2006; Dalla et al., 2007) and neuropsychiatric disorders (Elder et al., 2006). Interestingly, the proliferation and differentiation of the NSCs as well as the survival of newborn cells are dynamically influenced by a certain type of brain injuries such as ischemia (Sasaki et al., 2003), epilepsy (Takemiya et al., 2006) or neuroinflammation (Quin et al., 2007). Thus, the identification of the signaling molecules regulating NSC activity may contribute not only to the understanding of the neurogenesis mechanisms but also toward the development of new therapy against neural death.

Recently, lipopolysaccharide (LPS), a bacterial endotoxin, is reported to modulate the neurogenesis in the dentate gyrus of mammalian brain by causing the neuroinflammation including the activation of microglial cells. Ekdahl et al. (2003) and Monje et al. (2003) independently demonstrated that the peripheral administration of LPS diminishes the neurogenesis in the hippocampal dentate gyrus via the activation of microglial cells in the brain. The neurogenesis consists of the proliferation and the neural differentiation of the NSCs and the survival of newborn cells. However, it is not clear which processes of the neurogenesis are diminished by LPS. Also, the molecular mechanisms underlying the impairment of the neurogenesis elicited by systemic treatment with LPS are not fully understood. In general, the central and the peripheral actions of LPS are mediated or enhanced by the arachidonic acid cascade. In this cascade, two types of cyclooxygenase (COX), COX-1 and COX-2, act as rate-limiting enzymes catalyzing the conversion of arachidonic acid to prostaglandin H_2 (Bazan, 2001) and several prostanoids

0306-4522/08$32.00+0.00
doi:10.1016/j.neuroscience.2008.06.020

such as prostaglandin E_2 (PGE_2), prostaglandin$F_{2\alpha}$, prostaglandin I_2, prostaglandin D_2 (PGD_2) and thromboxane A_2 are known to be produced from prostaglandin H2 by specific synthetase (Nakahata, 2008). In addition, LPS is known to increase the expression level of COX-2 not only in the peripheral tissues but also in the brain (Bazan, 2001). On the other hand, COX and some prostanoids are reported to involve the modulation of the neurogenesis in the dentate gyrus by the ischemia (Sasaki et al., 2003) and the epilepsy (Jung et al., 2006). However, little is known about the involvement of COX in the modulatory actions of LPS on the neurogenesis in adult brains. This study was, therefore, designed to determine which processes of the neurogenesis in the adult mouse dentate gyrus are affected by LPS treatment and to clarify the involvement of COX in the LPS actions using the bromodeoxyuridine (BrdU) –pulse chase method and terminal deoxynucleotidyl transferase-mediated dUTP nick end-labeling (TUNEL) staining.

EXPERIMENTAL PROCEDURES

Animals

Adult male ICR mice (SLC, Shizuoka, Japan), 6 to 8-weeks-old at beginning of experiment, were used. All mice were housed in polypropylene cages (31×22×14 cm) with wood shavings, and were kept in an environment with a controlled temperature (23±2 °C) and light (12-h light/dark). Food and water were available *ad libitum*. All procedures were conducted in accordance with the guidelines of the Institution for Animal Care and the Use Committee of the Tohoku University. All experiments conformed to international guidelines on the ethical use of animals. All efforts were made to minimize the number of animals used and their suffering.

Drug treatment and sampling schedule

Mice received vehicle or various doses (0.1, 0.5 and 1 mg/kg i.p.) of LPS from *Escherichia coli* O111:B4 (Wako, Osaka, Japan). Five hours after LPS treatment, mice were intraperitoneally injected with BrdU (50 mg/kg; Nacalai Tesque, Kyoto, Japan) to label dividing cells. Two hours after BrdU injection, some mice were deeply anesthetized with diethyl ether and then, were perfused intracardially with 25 ml of chilled saline followed by 25 ml of 4% paraformaldehyde in 0.1 M phosphate buffer (PB) and thereafter their brains were quickly removed. The remaining mice were returned to their home cages and were maintained for 1, 7 or 21 days. Thereafter, animals were anesthetized and perfused as described above and their brains were quickly removed. In some experiments, mice were treated with the non-selective COX inhibitor indomethacin (10 mg/kg i.p., Wako), the selective COX-1 inhibitor SC-560 (12 mg/kg i.p., Cayman Chemical, Ann Arbor, MI, USA) or the selective COX-2 inhibitor NS-398 [10 mg/kg i.p. or 1 μg/10 μl saline/mouse i.c.v. injection, Wako] 1 h (i.p.) or 15 min (i.c.v.) before LPS injection. In one experiment, mice were first injected with BrdU (50 mg/kg i.p.) and received daily injection of LPS (1 mg/kg) for consecutive 7 days, which started 24 h after BrdU injection. Twenty-four hours after last LPS injection, their brains were sampled as described above.

Immunohistochemistry

The brains were post-fixed in 4% paraformaldehyde in 0.1 M PB overnight at 4 °C, followed by immersion in 20% sucrose in 0.1 M PB for 48 h. The brains were cut into 40 μm sections from the rostral to caudal edge of the dentate gyrus using a cryostat (MICROM HM560, Mikron Instrument, Inc., CA, USA) and the sections were alternately divided into two groups.

For BrdU-immunohistochemistry, one group of sections was treated with HCl (2 N) at 37 °C for 20 min, followed by neutralization with sodium borate buffer (0.15 M, pH 8.5) at room temperature for 10 min. After three washes with phosphate-buffered saline (PBS), the sections were incubated with rat anti-BrdU antibody (1:200; Oxford Biotechnology, Oxford, UK) diluted with phosphate-buffered saline containing 1% normal goat serum and 0.3% Triton X-100 (PBSGT) at 4 °C overnight, followed by Alexa Fluor® 568–conjugated goat anti-rat IgG (1:200; Molecular Probes, Eugene, OR, USA) and 1 μg/ml of Hoechst33258 for a nuclear counter staining, diluted with PBSGT at room temperature for 2 h. For the double-labeling of dentate gyrus, another group of the sections was processed for sequential immuno-staining using the following combination of primary antibody and appropriate second antibody; mouse anti–neuronal nuclei protein (NeuN) antibody (1:500, Chemicon, Temecula, CA, USA) followed by Alexa Fluor® 488–conjugated goat anti-mouse IgG (1:200; Molecular Probes), rabbit anti–glial fibrillary acidic protein (GFAP) antibody (1:150, Sigma-Aldrich, St. Louis, MO, USA) followed by Alexa Fluor® 488–conjugated goat anti-rabbit IgG (1:200; Molecular Probes), goat anti-doublecortin (DCX) antibody (1:100, Santa Cruz Biotechnology, Santa Cruz, CA, USA) followed by Alexa Fluor® 488–conjugated donkey anti-goat IgG (1:200; Molecular Probes), rabbit anti-COX-2 antibody (1:100, Cayman Chemical) followed by Alexa Fluor® 568–conjugated goat anti-rabbit IgG (1:200; Molecular Probes). Thereafter, the sections were mounted on slide glasses, dried and coverslipped with Gel/MountTM, aqueous mounting gel (Biomeda Corporation, Burlingame, CA, USA).

TUNEL staining

The effects of LPS on the cell death in the dentate gyrus were evaluated by TUNEL In Situ Cell Death Detection Kit, Fluorescein (Roche, Penzberg, Germany). The brains were post-fixed in 4% paraformaldehyde in 0.1 M PB overnight at 4 °C, followed by immersion in 20% sucrose in 0.1 M PB for 48 h and the hippocampus block was dissected out using scissors. The blocks were cut into 40 μm sections from the rostral to caudal edge of the dentate gyrus using a cryostat (MICROM HM560, Mikron Instrument, Inc.) and the sections were alternately divided into two groups. The sections were treated in Tris-buffered saline containing 0.15% Triton X-100 for 5 min and dehydrated in an ascending ethanol/distilled water series (30%, 70% and 95%, 5 min each), incubated in 100% ethanol (15 min), and gradually rehydrated (95%, 70% and 30%, 5 min each). The sections were then permeabilized with 0.1% Triton X-100 in 0.1% sodium citrate for 2 min on ice. After being washed with PBS three times, they were incubated with 100 μl TUNEL reaction mixture for 5 h at 37 °C. After being washed with PBS three times, the sections were incubated in PBS containing 1.25 μg/ml of Hoechst 33258 for 10 min at room temperature. After sequential washing with PBS and water, the slides were mounted on slide glasses, dried and coverslipped with Gel/MountTM, aqueous mounting gel (Biomeda Corporation).

Quantification of the number of BrdU-labeled cells and TUNEL-positive cells and the proportion of BrdU-labeled cells expressing cell type markers

BrdU-labeled cells and TUNEL-positive cells were counted using a 40× objective (IX70, Olympus, Tokyo, Japan) throughout the rostrocaudal extent of the dentate gyrus. For brains sampled 2 h after BrdU injection, we counted the number of BrdU-labeled cells in the SGZ, which was defined as a two-cell-body-wide zone (approximately 10 μm) along the border of the GCL and the hilus. For brains sampled 7 and 21 days after BrdU injection, we counted the number of BrdU-labeled cells in the SGZ and the

GCL. In TUNEL assay, we counted the number of positive cells in the SGZ and the GCL. Since we stained one of two section groups, resulting numbers were then multiplied by two to obtain the estimated total number of BrdU-labeled cells or TUNEL-positive cells per dentate gyrus. The counting was performed by an observer without any knowledge of the experimental groups.

The phenotype of the newly generated BrdU-labeled cells was analyzed by confocal scanning microscopy (TCS-NT, Leica Microsystems, Tokyo, Japan) and was expressed as the proportion, which was calculated by dividing the number of double-labeled cells by total number of BrdU-labeled cells in the SGZ and GCL.

Statistical analysis

The data in the present study were statistically analyzed by one-way ANOVA followed by Dunnett's test, Fisher's PLSD test or unpaired Student's *t*-test.

RESULTS

The effect of LPS treatment on the proliferation of the NSCs in the SGZ of the dentate gyrus

To determine whether LPS treatment affects the proliferation of the NSCs in the SGZ of the dentate gyrus, we quantified the number of BrdU-labeled cells in the SGZ of mice sampled 2 h after BrdU injection, since this procedure has been shown to be adequate to distinguish the proliferation from the survival of newborn cells (Mandyam et al., 2007). Fig. 1A shows the representative immunofluorescence images of BrdU-labeled cells in the SGZ of control (saline) and LPS-treated mice. LPS at doses of 0.1, 0.5 and 1 mg/kg did not affect the number of BrdU-labeled cells in the SGZ. There was no statistical difference in the number of BrdU-labeled cells in the SGZ between control and LPS-treated mice (Fig. 1B).

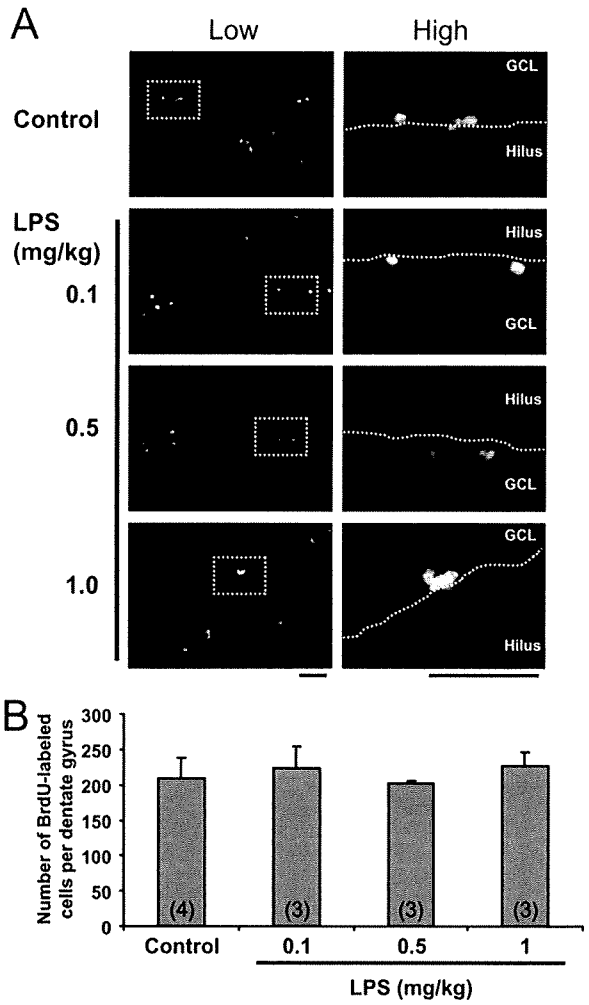

Fig. 1. The effects of LPS treatment on the number of BrdU-labeled cells in the SGZ 2 h after BrdU injection. (A) The representative immunofluorescence images of BrdU-labeled cells in the SGZ of mice treated with or without LPS. Mice were injected with BrdU 5 h after LPS treatment and their brains were sampled 2 h after BrdU injection. The left images represent entire dentate gyrus and right images are the enlargement of the SGZ enclosed by dashed rectangle in corresponding left images. Scale bar=50 μm. (B) The number of BrdU-labeled cells in the SGZ with or without LPS treatment (0.1, 0.5 and 1 mg/kg). Data represent the mean±S.E.M, and the number in parentheses indicates the number of animals.

The effect of LPS treatment on the survival of the newborn cells and the differentiation of the NSCs

We next investigated whether the treatment with LPS alters the survival of newborn cells in the dentate gyrus. We, therefore, quantified the number of BrdU-labeled cells in the SGZ as well as the GCL of control and LPS-treated mice at 7 and 21 days after the LPS treatment followed by BrdU injection, since the death of newly generated cells was reported to occur between 7 and 21 days after the terminal differentiation (Gould et al., 1999; Prickaerts et al., 2004; Mandyam et al., 2007). As shown in Fig. 2, LPS reduced the number of BrdU-labeled cell in the dentate gyrus 7 days after BrdU injection in a dose-dependent manner. The significant reduction in BrdU-labeled cell number was observed at 1.0 mg/kg of LPS (Fig. 2B). Twenty-one days after BrdU injection, the absolute number of BrdU in the dentate gyrus was lower than that at 7 days after BrdU injection (Figs. 2 and 3). The number of BrdU-labeled cells in the dentate gyrus 21 days after BrdU injection was dose-dependently reduced by LPS (Fig. 3B). The significant decrement in BrdU-labeled cell number was observed at 1.0 mg/kg of LPS (Fig. 3B). When we utilized a "pure" protocol to investigate the survival of newborn cells (Prickaerts et al., 2004) in which mice were first injected with BrdU (50 mg/kg i.p.) and then received daily injection of LPS (1 mg/kg) starting 24 h after BrdU injection for consecutive 7 days, LPS caused the significant decrease in the number of BrdU-labeled cells in the dentate gyrus [Control; 234.5±23.2 (n=4), LPS; 108.2±38.5 (n=4), P<0.05 (Student's *t*-test)].

As shown in Fig. 4, we observed that the systemic injection of LPS at 1 mg/kg significantly increased the number of TUNEL-positive cells in the dentate gyrus 5 days after the treatment, suggesting the LPS causes the cell death in the dentate gyrus.

To examine the effect of LPS on the fate of the NSCs, we next quantified the proportion of BrdU-labeled cells co-expressing the immature neuronal marker DCX, the mature neuronal marker NeuN or the astrocyte marker

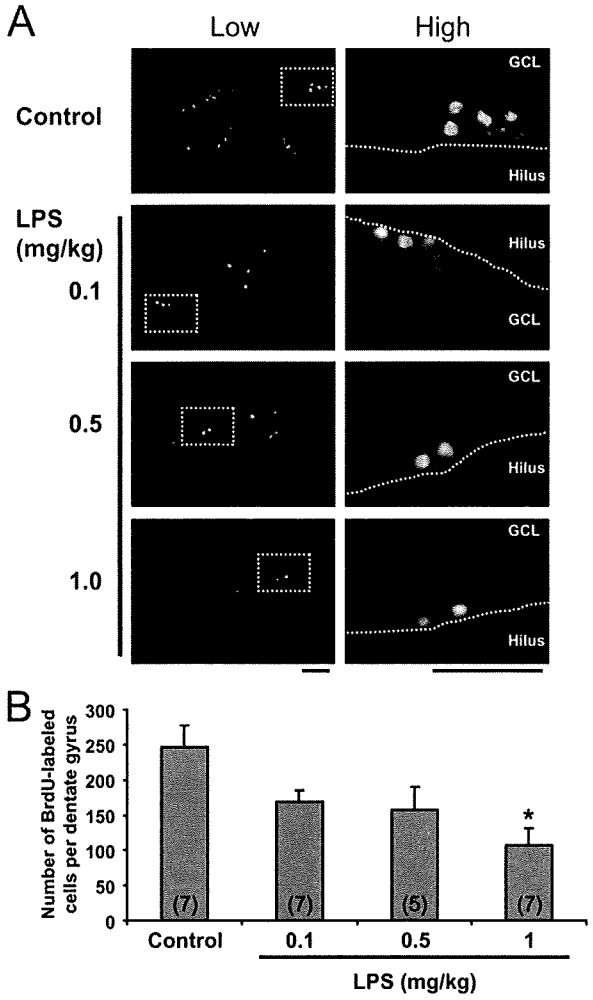

Fig. 2. The effects of LPS treatment on the number of BrdU-labeled cells in the dentate gyrus 7 days after BrdU injection. (A) The representative immunofluorescence images of BrdU-labeled cells in the dentate gyrus of mice treated with or without LPS. Mice were injected with BrdU 5 h after LPS treatment and their brains were sampled 7 days after BrdU injection. The left images represent entire dentate gyrus and right images are the enlargement enclosed by dashed rectangle in corresponding left images. Scale bar=50 μm. (B) The number of BrdU-labeled cells in the dentate gyrus. Data represent the mean±S.E.M, and the number in parentheses indicates the number of animals. The asterisk indicates a significant difference ($P<0.01$ vs. Control group, one-way ANOVA followed by Dunnett's test).

GFAP in the dentate gyrus 7 and 21 days after BrdU injection, respectively. Fig. 5A exhibits the representative confocal images double-immunostained with DCX and BrdU in the SGZ of mice sampled 7 days after BrdU injection. The majority of BrdU-labeled cells co-expressed DCX, and the proportion of DCX-positive cells among BrdU-labeled cells for control mice was 81.06±10.90%. LPS at doses up to 1.0 mg/kg failed to affect the proportion of DCX-positive cells (Fig. 5B). Fig. 5C and 5E shows the representative confocal images showing double-immunostaining of BrdU and NeuN, or BrdU and GFAP in the GCL of the dentate gyrus of mice sampled 21 days after BrdU injection, respectively. The majority of the BrdU-labeled cells co-expressed NeuN, while the BrdU-labeled cells with GFAP expression were sparsely observed. Fig. 5D and 5F shows the proportion of the cells double-labeled with NeuN and GFAP in the GCL, respectively. No difference was observed in the proportion of the BrdU-labeled cells co-expressing either NeuN or GFAP between groups.

The effects of COX inhibitors on LPS-induced impairment of the newborn cell survival in the dentate gyrus

We examined the effects of the pretreatment with COX inhibitors on LPS-induced impairment of the newborn cell survival in the dentate gyrus by quantifying the number of BrdU-labeled cells in the SGZ and the GCL 7 days after

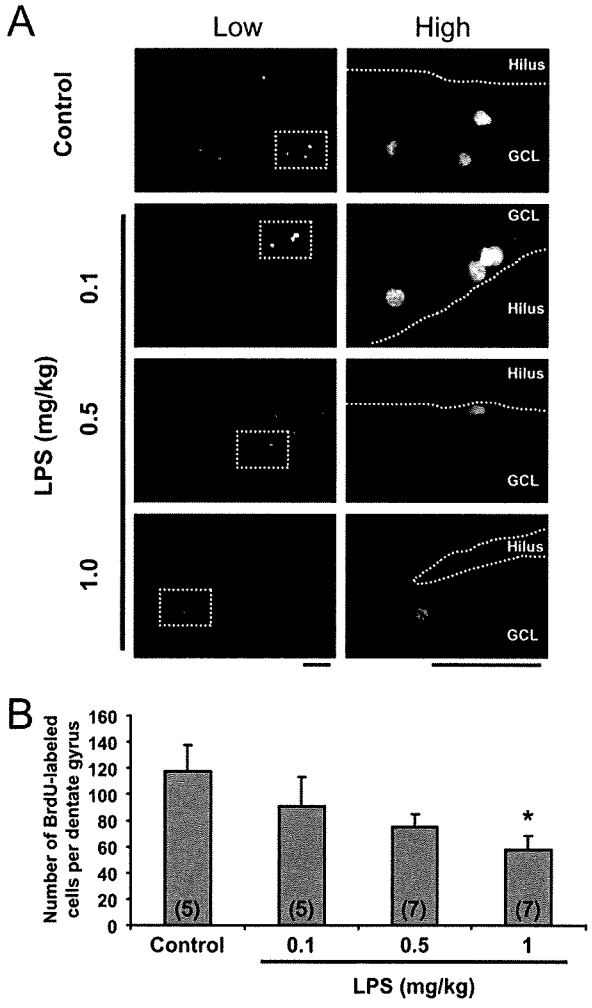

Fig. 3. The effects of LPS treatment on the number of BrdU-labeled cells in the dentate gyrus 21 days after BrdU injection. (A) The representative immunofluorescence images of BrdU-labeled cells in the dentate gyrus of mice treated with or without LPS. Mice were injected with BrdU 5 h after LPS treatment and their brains were sampled 21 days after BrdU injection. The left images represent the entire dentate gyrus and right images are the enlargement enclosed by a dashed rectangle in the corresponding left images. Scale bar=50 μm. (B) The number of BrdU-labeled cells in the dentate gyrus. Data represent the mean±S.E.M, and the number in parentheses indicates the number of animals. The asterisk indicates a significant difference ($P<0.01$ vs. Control group, one-way ANOVA followed by Dunnett's test).

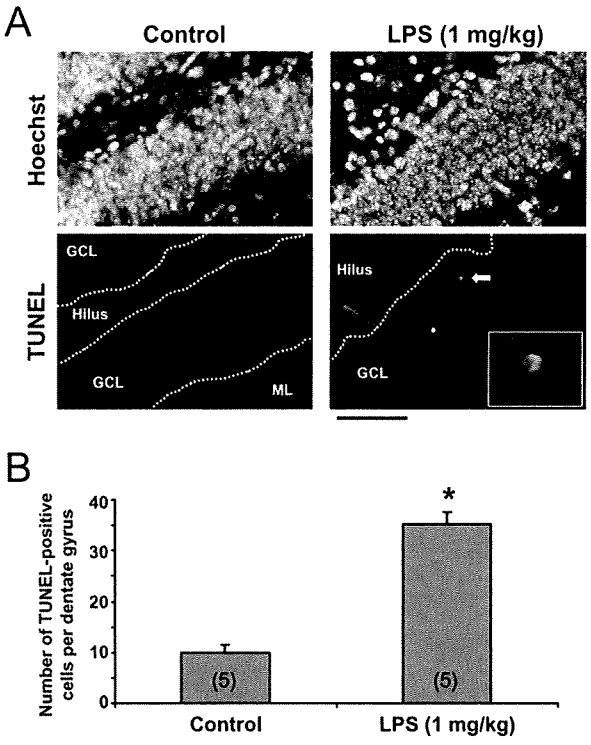

Fig. 4. The effects of LPS treatment on the number of TUNEL-positive cells in the dentate gyrus 5 days after LPS injection. (A) The representative immunofluorescence images of Hoechst33258-staining and TUNEL-positive cells in the dentate gyrus of mice treated with or without LPS (1 mg/kg). Mice were injected with LPS (1 mg/kg) and their brains were sampled 5 days after. The inset image in TUNEL staining of LPS group is an enlargement of TUNEL-positive cells indicated by an arrow. Scale bar=50 μm. (B) The number of TUNEL-positive cells in the GCL. Data represent the mean±S.E.M, and the number in parentheses indicates the number of animals. The asterisk indicates a significant difference ($P<0.05$ vs. Control group, Student's *t*-test).

BrdU injection. One-way ANOVA revealed the significant effects of treatment [$F(4, 26)=6.155$, $P<0.01$] (Fig. 6A). The systemic injection of LPS (1 mg/kg) decreased the number of BrdU-labeled cells compared with control group. The systemic injection of indomethacin (10 mg/kg), a non-selective COX inhibitor, completely protected LPS-induced reduction in BrdU-labeled cell number in the dentate gyrus (Fig. 6A). The systemic injection of NS-398 (10 mg/kg), a selective COX-2 inhibitor, also completely blocked the decrement in BrdU-labeled cell number elicited by LPS (Fig. 6A). These protective effects of inhibitors were confirmed by post hoc Fisher's PLSD test revealing that there was significant difference between control and LPS+saline group, but not between control and LPS+indomethacin group, and not between control and LPS+NS-398 group. Indomethacin or NS-398 did not affect the basal number of BrdU-labeled cells in mice without LPS treatment (data not shown). In contrast, LPS-induced reduction in BrdU-labeled cell number was unaffected by the pretreatment with SC-560 (12 mg/kg), a selective COX-1 inhibitor. Furthermore, as shown in Fig. 6B, i.c.v. injection of NS-398 (1 μg/10 μl/mouse) also completely protected against LPS-induced decrement in BrdU-labeled cell number, since there was significant difference between control and LPS+saline group, but not between control and LPS+NS-398 group (post hoc Fisher's PLSD test) (Fig. 6B). I.c.v. injection of NS-398 itself did not affect the basal number of BrdU-labeled cells in mice without LPS treatment (Fig. 6B).

Expression of COX-2 in the dentate gyrus after LPS treatment

Finally, we investigated the expression of COX-2 in the dentate gyrus of mice with or without LPS treatment. Seven hours after LPS injection (1 mg/kg), it significantly increased the number of COX-2-positive cells in the GCL and the molecular layer (ML) (Fig. 7A). Even 7 days after LPS injection (1 mg/kg), it caused the moderate, but significant increase in the number of COX-2-positive cells in the GCL, but in the ML (Fig. 7A). The immunohistochemistry of double-immunostaining for COX-2 and specific cell type markers revealed that the majority of COX-2-positive cells in the GCL co-expressed NeuN and the small portion of COX-2-positive cells in the GCL co-expressed DCX (Fig. 7C and 7D). It was noteworthy that DCX- and COX-2-double positive cells exist only in the GCL, but not in the SGZ (Fig. 7D). In control mice, COX-2 expression is not detectable in vascular associated cells in the dentate gyrus, however, numerous COX-2 immunoreactive cells were found 7 h and 7 days after LPS administration (data not shown). There were no COX-2-positive cells in the SGZ and the hilus of mice with or without LPS treatment (data not shown).

DISCUSSION

The present study was designed to examine the effects of LPS, a bacterial endotoxin, on the neurogenesis in the dentate gyrus of adult mice and to clarify the involvement of COX in the LPS actions. Using the BrdU–pulse chase method and TUNEL method, we found that LPS diminished the neurogenesis in the dentate gyrus of adult mice by impairing the survival of newborn cells and these effects of LPS were mediated by COX-2 in the brain. To our knowledge, this is the first report to show the involvement of COX-2 in the brain in the impairment of the neurogenesis in the hippocampal dentate gyrus by LPS.

The neurogenesis in the adult dentate gyrus is a complex of multi-step process, in which the immature NSCs proliferate and then differentiate into three neural cell lineages and the limited number of newborn cells survive thereafter (Reynolds et al., 1992; Kempermann et al., 2004). Since the cell cycle length of NSCs in the dentate gyrus of adult mice is reported to be approximately 14 h (Mandyam et al., 2007), the proliferation of the NSCs should be investigated using a protocol in which mice are treated with a tracer (BrdU) and killed maximally within 24 h (Prickaerts et al., 2004). Thus, our protocol of the sampling 2 h after BrdU injection enables us to exclude the contribution of the newborn cell survival and to examine the proliferation itself. On the other hand, the number of BrdU-labeled cells in the dentate gyrus was reported to decline between 1 and 2 weeks in rats (Gould et al., 1999) and between 24 h and 4 weeks in mice (Mandyam et al.,

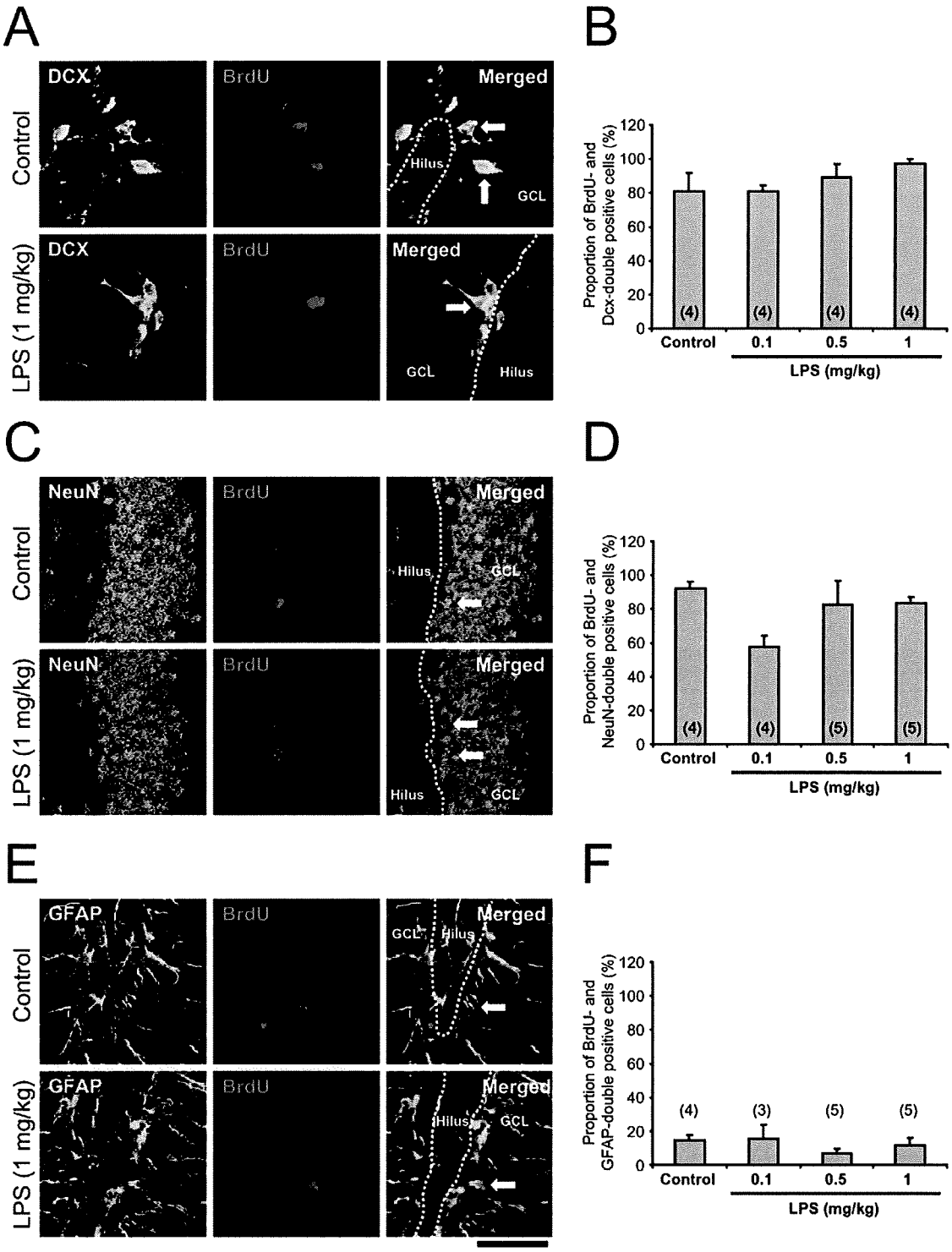

Fig. 5. The effects of LPS treatment on the proportion of DCX-, NeuN- or GFAP-positive cells among BrdU-labeled cells in the dentate gyrus. Representative confocal images of the double labeling of BrdU-labeled cells with the immature neural marker DCX (A), the mature neural marker NeuN (C) and the astrocyte marker GFAP (E) in the dentate gyrus of mice treated with or without LPS, 7 days (A; DCX) and 21 days (C; NeuN, E; GFAP) after BrdU injection. The arrows in the merged image indicate double-positive cells. Scale bar=50 μm. The proportion of BrdU and DCX (B), NeuN (D) or GFAP (F) double-positive cells in the dentate gyrus, 7 days (B; DCX) and 21 days (D; NeuN, F; GFAP) after BrdU injection. Data represent the mean±S.E.M, and the number in parentheses indicates the number of animals.

2007) without the change in the labeling intensity per cell, suggesting that the death of newborn cells in the rodent dentate gyrus occurs during this period. These reports taken together with our finding that LPS decreased the

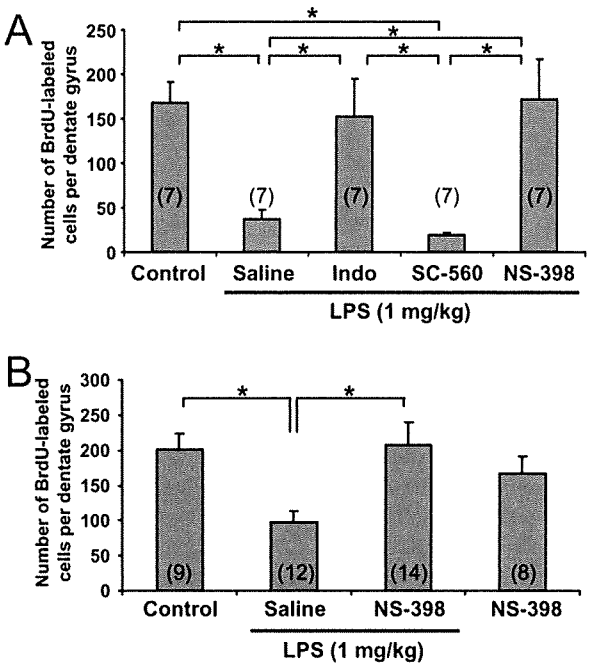

Fig. 6. The effects of COX inhibitors on LPS-induced impairment of the newborn cell survival in the dentate gyrus. (A) The effect of systemic injection of COX inhibitors on LPS-induced decrement in BrdU-labeled cell number in the dentate gyrus 7 days after BrdU injection. Indo (10 mg/kg), SC-560 (12 mg/kg) or NS-398 (10 mg/kg) was injected to mice 1 h before LPS treatment and BrdU was given 5 h after LPS injection. Their brains were sampled 7 days after BrdU injection. Indo, indomethacin. (B) The effect of central injection of a selective COX-2 inhibitor, NS-398, on LPS-induced decrement in BrdU-labeled cell number in the dentate gyrus 7 days after BrdU injection. The inhibitors were injected to mice 15 min before LPS treatment and their brains were sampled 7 days after BrdU injection. Data represent the mean±S.E.M, and the number in parentheses indicates the number of animals. * Significant difference ($P<0.05$, one-way ANOVA followed by Fisher's PLSD test).

number of BrdU-labeled cells 7 and 21 days, but not 2 h, after BrdU injection suggest that the survival of newborn cells in the dentate gyrus is negatively regulated by the systemic treatment with LPS. Our results of TUNEL staining also suggested that LPS decreased the cell survival in the dentate gyrus. The significant decrease in the number of BrdU-labeled cells in the dentate gyrus observed using a "pure" protocol investigating the newborn cell survival (Prickaerts et al., 2004) also support this idea. We also found that the proportion of cells committed to neural lineage (DCX- and NeuN-positive) and astroglial lineage (GFAP-positive) was not changed by LPS treatment, suggesting that LPS does not affect the differentiation process itself. LPS, therefore, might reduce the survival of immature cells that do not undergo the fate-determination. Alternatively, we cannot rule out the possibility that LPS decreases the survival of neuron-restricted progenitor cells and astrocyte-restricted progenitor cells in the same degree. Since recent studies revealed that neurogenesis in the adult dentate gyrus is the sequential maturation from several subtypes of dividing cells (nestin-positive type-1 and type-2 cells and DCX-positive type-3 cells) into several subtypes of postmitotic cells (calretinin- or NeuN-positive cells) (Fukuda et al., 2003; Kronenberg et al., 2003; Jessberger et al., 2005), further experiments will be required to confirm which types of newly generated cells are affected by LPS treatment.

Recently, it was demonstrated that the neural stem/progenitor cells in the dentate gyrus abundantly express Toll-like receptor four (TLR4) known as a LPS receptor and the treatment with LPS directly diminished the proliferation

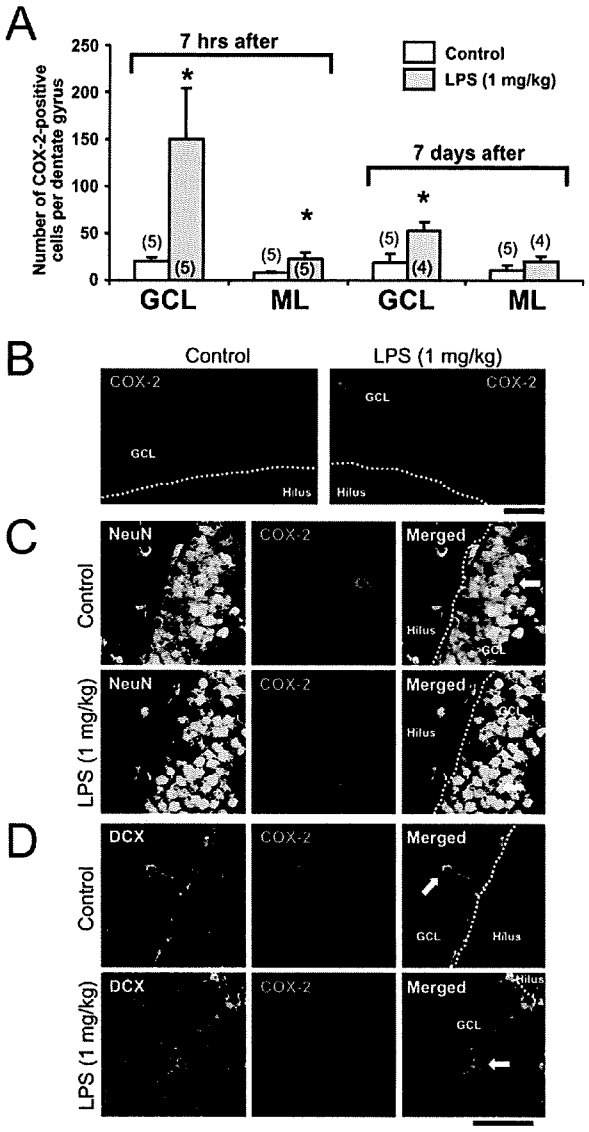

Fig. 7. The expression of COX-2 in the dentate gyrus. (A) The number of COX-2-positive cells in the GCL and ML of the dentate gyrus of mice 7 h and 7 days after the treatment with or without LPS. The number in parentheses indicates the number of animals. The asterisk indicates a significant difference ($P<0.01$ vs. Saline group, Student's *t*-test). (B) Representative immunofluorescence images of COX-2 positive cells in the dentate gyrus of mice 7 days after the treatment with or without LPS. The arrows in the merged image indicate double-positive cells. Scale bar=50 μm. Representative confocal images of the double labeling of COX-2 positive cells with the neural marker NeuN (C) and the immature neural marker DCX (D) in the dentate gyrus of mice 7 days after treatment with or without LPS. The arrows in the merged image indicate double-positive cells. Scale bar=50 μm.

of cultured neural stem/progenitor cells in an NF-κB-dependent mechanism (Rolls et al., 2007). It has been demonstrated, however, that LPS (up to 0.1 μg/ml) failed to affect the survival of cultured neural stem/progenitor cells under *in vitro* conditions (Rolls et al., 2007). In marked contrast, it is reported that treatment with LPS (0.1 μg/ml) induced apoptosis in hippocampus-derived NSCs (Chiou et al., 2006; Huang et al., 2007). Because it is unknown whether LPS injected intraperitoneally at doses up to 1 mg/kg would pass through the brain–blood barrier and reach the plasma membrane of the NSCs, the impairment of newborn cell survival observed in the present study might be caused by indirect actions of LPS via COX-2 as described below.

One of the novel findings in the present study is that LPS-induced impairment of the newborn cell survival was ameliorated not only by the systemic injection of either a non-selective COX inhibitor (indomethacin) or a COX-2 selective inhibitor (NS-398), but also by the central injection of NS-398, suggesting the implication of brain COX-2 in the LPS actions. There were some previous reports indicating the roles of COX-2 in the modulation of the neurogenesis in the dentate gyrus by a certain types of brain injury. Sasaki et al. (2003) demonstrated that ischemia-induced enhancement of the NSC proliferation in the dentate gyrus was blunted by treatment with indomethacin or NS-398 or in COX-2-deficient mice (Sasaki et al., 2003). Furthermore, ectopic neurogenesis in the hippocampus elicited by the epilepsy was shown to be inhibited by a COX-2 inhibitor, celecoxib (Jung et al., 2006). These facilitatory roles of COX-2 in injury-induced neurogenesis are quite opposite to the suppressive roles of COX-2 in LPS-induced diminishment of the neurogenesis in the dentate gyrus. The difference in the spatial pattern and the levels of COX-2 expression between brain injury (ischemia or epilepsy) and LPS treatment may account for these opposite roles of COX-2. Under our experimental condition, COX-2 expression in control mice was seen in the GCL, but not in the SGZ containing the immature NSCs. These expression patterns of COX-2 in the dentate gyrus are consistent with previous reports (Sasaki et al., 2003; Takemiya et al., 2006). We also demonstrated that the systemic injection of LPS (1 mg/kg) increased the expression of COX-2 in the GCL and the blood vessels, but not in the hilus. In contrast, ischemia has been shown to increase COX-2 expression in the reactive astrocytes located in the hilus (Sasaki et al., 2003). Thus, the difference in COX-2-expressing cell type as well as the expression levels may explain the opposite actions of brain injury (ischemia or epilepsy) and LPS on neurogenesis in the dentate gyrus.

Although COX-2 may modulate the neurogenesis in the dentate gyrus through generation of prostaglandins and PGE_2, and is already reported to modulate neurogenesis in the dentate gyrus (Uchida et al., 2002), it remained unclear which type(s) of prostaglandins plays a critical role in LPS-induced impairment of neurogenesis. Interestingly, the central infusion of LPS drastically increases the brain levels of PGD_2, a major metabolite of arachidonic acid in the CNS (Rosenberger et al., 2004). In addition, it is suggested that the cyclopentenone 15-deoxy-prostaglandin J_2 (15d-PGJ_2), which is non-enzymatically converted from PGD_2 (Shibata et al., 2002), induces apoptosis of a variety of cell types including the oligodendrocyte precursor cells in a peroxisome proliferators-activated receptor γ-dependent and -independent mechanism (Xiang et al., 2007). Thus, PGD_2, as well as its metabolite 15d-PGJ_2, is a feasible candidate mediating LPS action in neurogenesis.

LPS is generally known as a phlogistic agent to induce neuroinflammation (Ekdahl et al., 2003; Rosenberger et al., 2004; Rolls et al., 2007) and the activation of microglial cells is one of typical phenomena elicited by LPS treatment (Quin et al., 2007). It has been reported that the activation of microglial cells mediates LPS-induced diminishment of neurogenesis in the dentate gyrus via IL-6 (Monje et al., 2003) or TNF-α (Liu et al., 2005) secretion from the activated microglial cells (Ekdahl et al., 2003). In addition, LPS is known to increase the blood levels of interleukin-1β, which in turn increased the gene expression of COX-2 in the blood vessel cells in the brain (Fantuzzi and Dinarello, 1999; Bazan, 2001; Blais et al., 2005; Quan and Banks, 2007). Furthermore, LPS is known to increase the brain levels of interleukin-1β (Fantuzzi and Dinarello, 1999), which is shown to reduce neurogenesis in the dentate gyrus (Goshen et al., 2008; Koo and Duman, 2008; Spulber et al., 2008). Since COX-2 activation is known to be directly or indirectly involved in a wide variety of these neuroinflammation processes elicited by LPS (Minghetti, 2004; Quin et al., 2007), the ameliorating effects of COX-2 inhibitor against LPS action might be exerted by suppressing the cytokine production involved in neuroinflammation. Further experiments will be required to confirm this possibility.

Acknowledgments—This research was supported by a Grant-in-Aid for Scientific Research on Priority Areas (18057002) to N.N., Grant-in-Aid for Exploratory Research (19659011) to N.N. and Grant-in-Aid for Exploratory Research (19659055) to T.M.

REFERENCES

Aimone JB, Wiles J, Gage FH (2006) Potential role for adult neurogenesis in the encoding of time in new memories. Nat Neurosci 9:723–727.

Bazan NG (2001) COX-2 as a multifunctional neuronal modulator. Nat Med 7:414–415.

Blais V, Turrin NP, Rivest S (2005) Cyclooxygenase 2 (COX-2) inhibition increases the inflammatory response in the brain during systemic immune stimuli. J Neurochem 95:1563–1574.

Cameron HA, McKay RD (2001) Adult neurogenesis produces a large pool of new granule cells in the dentate gyrus. J Comp Neurol 435:406–417.

Chiou SH, Chen SJ, Peng CH, Chang YL, Ku HH, Hsu WM, Ho LL, Lee CH (2006) Fluoxetine up-regulates expression of cellular FLICE-inhibitory protein and inhibits LPS-induced apoptosis in hippocampus-derived neural stem cell. Biochem Biophys Res Commun 343:391–400.

Christie BR, Cameron HA (2006) Neurogenesis in the adult hippocampus. Hippocampus 16:199–207.

Dalla C, Bangasser DA, Edgecomb C, Shors TJ (2007) Neurogenesis and learning: acquisition and asymptotic performance predict how

many new cells survive in the hippocampus. Neurobiol Learn Mem 88:143–148.
Ekdahl CT, Claasen JH, Bonde S, Kokaia Z, Lindvall O (2003) Inflammation is detrimental for neurogenesis in adult brain. Proc Natl Acad Sci U S A 100:13632–13637.
Elder G, De Gasperi R, Gama Sosa M (2006) Neurogenesis in adult brain and Neuropsychiatric disorders. Mt Sinai J Med 73:931–940.
Fantuzzi G, Dinarello CA (1999) Interleukin-18 and interleukin-1 beta: two cytokine substrates for ICE (caspase-1). J Clin Immunol 19: 1–11.
Fukuda S, Kato F, Tozuka Y, Yamaguchi M, Miyamoto Y, Hisatsune T (2003) Two distinct subpopulations of nestin-positive cells in adult mouse dentate gyrus. J Neurosci 23:9357–9366.
Gage FH (2002) Neurogenesis in the adult brain. J Neurosci 22: 612–613.
Goshen I, Kreisel T, Ben-Menachem-Zidon O, Licht T, Weidenfeld J, Ben-Hur T, Yirmiya R (2008) Brain interleukin-1 mediates chronic stress-induced depression in mice via adrenocortical activation and hippocampal neurogenesis suppression. Mol Psychiatry 13:717–728.
Gould E, Beylin A, Tanapat P, Reeves A, Shors TJ (1999) Learning enhances adult neurogenesis in the hippocampal formation. Nat Neurosci 2:260–265.
Gould E, Tanapat P, Rydel T, Hastings N (2000) Regulation of hippocampal neurogenesis in adulthood. Biol Psychiatry 48:715–720.
Huang YY, Peng CH, Yang YP, Wu CC, Hsu WM, Wang HJ, Chan KH, Chou YP, Chen SJ, Chang YL (2007) Desipramine activated Bcl-2 expression and inhibited lipopolysaccharide-induced apoptosis in hippocampus-derived adult neural stem cells. J Pharmacol Sci 104:61–72.
Jessberger S, Romer B, Babu H, Kempermann G (2005) Seizures induce proliferation and dispersion of doublecortin-positive hippocampal progenitor cells. Exp Neurol 196:342–351.
Jung KH, Chu K, Lee ST, Kim J, Sinn DI, Kim JM, Park DK, Lee JJ, Kim SU, Kim M, Lee SK, Roh JK (2006) Cyclooxygenase-2 inhibitor, celecoxib, inhibits the altered hippocampal neurogenesis with attenuation of spontaneous recurrent seizures following pilocarpine-induced status epilepticus. Neurobiol Dis 23:237–246.
Kempermann G, Wiskott L, Gage FH (2004) Functional significance of adult neurogenesis. Curr Opin Neurobiol 14:186–191.
Koo JW, Duman RS (2008) IL-1beta is an essential mediator of the antineurogenic and anhedonic effects of stress. Proc Natl Acad Sci U S A 105:751–756.
Kronenberg G, Reuter K, Steiner B, Brandt MD, Jessberger S, Yamaguchi M, Kempermann G (2003) Subpopulations of proliferating cells of the adult hippocampus respond differently to physiologic neurogenic stimuli. J Comp Neurol 467:455–463.
Liu YP, Lin HI, Tzeng SF (2005) Tumor necrosis factor-alpha and interleukin-18 modulate neuronal cell fate in embryonic neural progenitor culture. Brain Res 1054:152–158.
Mandyam CD, Harburg GC, Eisch AJ (2007) Determination of key aspects of precursor cell proliferation, cell cycle length and kinetics in the adult mouse subgranular zone. Neuroscience 146:108–122.
Minghetti L (2004) Cyclooxygenase-2 (COX-2) in inflammatory and degenerative brain diseases. J Neuropathol Exp Neurol 63: 901–910.
Monje ML, Toda H, Palmer TD (2003) Inflammatory blockade restores adult hippocampal neurogenesis. Science 302:1760–1765.
Nakahata N (2008) Thromboxane A_2: Physiology/pathophysiology, cellular signal transduction and pharmacology. Pharmacol Ther 118:18–35.
Ono K, Kagawa T, Tsumori T, Yokota S, Yasui Y (2001) Morphological changes and cellular dynamics of oligodendrocyte lineage cells in the developing vertebrate central nervous system. Dev Neurosci 23:346–355.
Prickaerts J, Koopmans G, Blokland A, Scheepens A (2004) Learning and adult neurogenesis: survival with or without proliferation? Neurobiol Learn Mem 81:1–11.
Quan N, Banks WA (2007) Brain-immune communication pathways. Brain Behav Immun 21:727–735.
Quin L, Wu X, Block M, Breese G, Hong J, Knapp D, Crews F (2007) Systemic LPS causes chronic neuroinflammation and progressive neurodegeneration. Glia 55:453–462.
Reynolds BA, Tetzlaff W, Weiss S (1992) A multipotent EGF-responsive striatal embryonic progenitor cell produces neurons and astrocytes. J Neurosci 12:4565–4574.
Rolls A, Shechter R, London A, Ziv Y, Ronen A, Levy R, Schwartz M (2007) Toll-like receptors modulate adult hippocampal neurogenesis. Nat Cell Biol 9:1081–1088.
Rosenberger TA, Villacreses NE, Hovda JT, Bosetti F, Weerasinghe G, Wine RN, Harry GJ, Rapoport SI (2004) Rat brain arachidonic acid metabolism is increased by a 6-day intracerebral ventricular infusion of bacterial lipopolysaccharide. J Neurochem 88:1168–1178.
Sasaki T, Kitagawa K, Sugiura S, Omura-Matsuoka E, Tanaka S, Yagita Y, Okano H, Matsumoto M, Hori M (2003) Implication of cyclooxygenase-2 on enhanced proliferation of neural progenitor cells in the adult mouse hippocampus after ischemia. J Neurosci Res 72:461–471.
Shibata T, Kondo M, Osawa T, Shibata N, Kobayashi M, Uchida K (2002) 15-Deoxy-delta 12,14-prostaglandin J2. A prostaglandin D2 metabolite generated during inflammatory processes. J Biol Chem 277:10459–10466.
Shors TJ, Miesegaes G, Beylin A, Zhao M, Rydel T, Gould E (2001) Neurogenesis in the adult is involved in the formation of trace memories. Nature 410:372–376.
Spulber S, Oprica M, Bartfai T, Winblad B, Schultzberg M (2008) Blunted neurogenesis and gliosis due to transgenic overexpression of human soluble IL-1ra in the mouse. Eur J Neurosci 27:549–558.
Takemiya T, Maehara M, Matsumura K, Yasuda S, Sugiura H, Yamagata K (2006) Prostaglandin E2 produced by late induced COX-2 stimulates hippocampal neuron loss after seizure in the CA3 region. Neurosci Res 56:103–110.
Uchida K, Kumihashi K, Kurosawa S, Kobayashi T, Itoi K, Machida T (2002) Stimulatory effects of prostaglandin E2 on neurogenesis in the dentate gyrus of the adult rat. Zoolog Sci 19:1211–1216.
Xiang Z, Lin T, Reeves SA (2007) 15d-PGJ2 Induces apoptosis of mouse oligodendrocyte precursor cells. J Neuroinflammation 4:18.

(Accepted 6 June 2008)
(Available online 17 June 2008)

The FASEB Journal • Research Communication

Cholecystokinin-A receptors regulate photic input pathways to the circadian clock

Takao Shimazoe,* Mitsutaka Morita,* Shinichiro Ogiwara,† Tomoyoshi Kojiya,† Junpei Goto,† Masaki Kamakura,‡ Takahiro Moriya,§ Kazuyuki Shinohara,§ Soichi Takiguchi,‖ Akira Kono,‖ Kyoko Miyasaka,¶ Akihiro Funakoshi,‖ and Masayuki Ikeda†,#,1

*Graduate School of Pharmaceutical Sciences, Kyushu University, Fukuoka, Japan; †Graduate School of Science and Engineering, University of Toyama, Toyama, Japan; ‡Biotechnology Research Center, Faculty of Engineering, Toyama Prefectural University, Toyama, Japan; §Department of Translational Medical Sciences, Course of Medical and Dental Sciences, Nagasaki University Graduate School of Biomedical Sciences, Nagasaki, Japan; ‖National Kyushu Cancer Center, Fukuoka, Japan; ¶Department of Translational Medical Sciences, Tokyo Metropolitan Institute of Gerontology, Tokyo, Japan; and #Advanced Institute for Biological Science, Waseda University, Tokyo, Japan

ABSTRACT **Daily behaviors are strongly dominated by internally generated circadian rhythms, but the underlying mechanisms remain unclear. In mammals, photoentrainment of behaviors to light-dark cycles involves signaling from both intrinsically photosensitive retinal ganglion cells and classic photoreceptor pathways to the suprachiasmatic nucleus (SCN). How classic photoreceptor pathways work with the photosensitive ganglion cells, however, is not fully understood. Although cholecystokinin (CCK) peptide has been shown to be present in a variety of vertebrate retinas, its function at a systems level is also unknown. In the present study we examined a possible role of CCK-A receptors in photoentrainment using CCK-A receptor knockout mice. The lacZ reporter gene within a gene-knockout cassette revealed precise localization of CCK-A receptors in the circadian clock system. We demonstrated that CCK-A receptors were located predominately on glycinergic amacrine cells but were rarely found on SCN neurons. Moreover, Ca^{2+} imaging analysis demonstrated that the CCK-A agonist, CCK-8 sulfate (CCK-8s), mobilized intracellular Ca^{2+} in amacrine cells but not glutamate-receptive SCN neurons. Furthermore, light pulse-induced *mPer1/mPer2* gene expression in SCN, behavioral phase shifts, and the pupillary reflex were significantly reduced in CCK-A receptor knockout mice. These data indicate a novel function of CCK-A receptors in the nonimage-forming photoreception presumably *via* amacrine cell-mediated signal transduction pathways.—Shimazoe, T., Morita, M., Ogiwara, S., Kojiya, T., Goto, J., Kamakura, M., Moriya, T., Shinohara, K., Takiguchi, S., Kono, A., Miyasaka, K., Funakoshi, A., Ikeda, M. Cholecystokinin-A receptors regulate photic input pathways to the circadian clock. *FASEB J.* 22, 1479–1490 (2008)**

Key Words: cholecystokinin-A receptor mutant mice · glycinergic amacrine cells · melanopsin retinal ganglion cells · suprachiasmatic nucleus neurons

DAILY BEHAVIORAL RHYTHMS are strictly controlled by the hypothalamic suprachiasmatic nucleus (SCN), the mammalian circadian pacemaker (1, 2). Although these rhythms persist under time cue-free conditions, they are usually synchronized to the environmental light-dark cycles, a process called photoentrainment. The classic photoreceptor cells, rods and cones, are not the only cells involved in this process, however, because photoentrainment still occurs in mutant (*rdta/cl*) mice lacking all rods and cones (3). It has been shown that intrinsically photosensitive retinal ganglion cells, which contain the pigment melanopsin (4), respond directly to light and send monosynaptic projections to the SCN and the olivary pretectal nuclei, as part of nonimage-forming visual functions including photoentrainment and the pupillary light reflex (5, 6). Photoentrainment is still possible, however, in melanopsin-deficient ($Opn4^{-/-}$) mice and only becomes absent with the subtraction of both the photosensitivity of retinal ganglion cells and classic photoreceptors in double mutant melanopsin-deficient and retinal degeneration ($Opn4^{-/-}$; *rd/rd*) mice (7). These results suggest that classic photoreceptors and intrinsically photosensitive retinal ganglion cells represent compensatory photoreception mechanisms for circadian photoentrainment. In mice, intrinsically photosensitive retinal ganglion cell dendrites in the inner ON region of the inner plexiform layer receive both bipolar and amacrine cell terminals, whereas intrinsically photosensitive retinal ganglion cell dendrites stratifying in the outer OFF region of the inner plexiform layer receive only amacrine cell terminals (8). The circuitry between photoreceptor pathways, retinal ganglion cells, and amacrine cells underlying photoentrainment, however, is not fully understood.

In SCN neurons, some subcellular responses have been identified that may be involved in photoentrainment. After photic stimulation at night, retino-recipient SCN neurons respond to glutamate release from reti-

[1] Correspondence: Department of Biology, Faculty of Science, University of Toyama, Rm. B214, 3190 Gofuku, Toyama-city, Toyama 930-8555, Japan. E-mail: msikeda@sci.u-toyama.ac.jp

doi: 10.1096/fj.07-9372com

nohypothalamic tract terminals with an activation of *N*-methyl-D-aspartate glutamate receptors, an increase in cytosolic Ca^{2+} concentration, and immediate expression of clock genes, such as *mPer1* and *mPer2* (9–11). Several other signaling mechanisms also appear to be involved. For example, pituitary adenylate cyclase-activating polypeptide is released from retinohypothalamic tract terminals in addition to glutamate (12), and serotonin-1B receptors (13) and GABA-B receptors (14) on retinohypothalamic tract terminals may synergistically control neurotransmitter release on SCN pacemaker neurons. The interconnections of these elements remain unclear, however.

Cholecystokinin (CCK) is one of the most abundant neuropeptides in the central nervous system, but its function in many pathways has not been identified. CCK immunoreactive cell bodies and axons have been shown to be sparsely dispersed throughout the SCN of rats, mice, and hamsters (6, 15–17). In addition, CCK peptide has been shown to be present in a variety of vertebrate retinas (18–21). In rat retinas, it is located predominantly in amacrine cells (22) and may function for local signal transduction pathways, as expression of CCK-A and CCK-B receptor mRNAs has been reported for retinal homogenates (23). The function of CCK within this circadian clock circuitry has not been elucidated, but it is a reasonable hypothesis that CCK peptides have a role in the SCN clock work itself and/or photic input pathways to the SCN. Indeed, we have reported that photoentrainment of locomotor rhythms and immediate early gene (c-*fos*) expression in SCN neurons in response to light are significantly reduced in Otsuka Long Evans Tokushima Fatty (OLETF) rats, a strain of obese mutant rats, that lack CCK-A receptor genes (24–27). Although these data are highly suggestive, multiple other genes are also lacking in OLETF rats; thus, further experiments are needed to identify the specific gene responsible for the circadian photoentrainment (28, 29).

To examine the specific function of CCK-A receptors in the circadian clock system, in the present study we used mutant mice lacking CCK-A receptors ($CCKAR^{-/-}$) that carry the lacZ reporter gene within a gene-knockout cassette (30), which allowed precise study of the localization of CCK-A receptors. We also examined the function of these receptors at the gene expression, intracellular signaling, and behavioral levels. Based on these data, we propose that CCK-A receptors on a subpopulation of retinal amacrine cells may have an important role in nonimage-forming visual functions.

MATERIALS AND METHODS

Mice

Male $CCKAR^{-/-}$ mice and their wild-type control littermates were generated as described previously (30). In short, the targeting vector was designed to replace the *SalI-BglII* 1.9-kb genomic fragment of the mouse CCK-A receptor gene with a NLS-lacZ and pGK-neo cassette. The homologous recombination deleted the first 122 amino acids, including the first membrane-spanning region of the CCK-A receptor. J1 embryonic stem (ES) cells were electroporated with the targeting vector and selected with G418 on embryonic fibroblast feeder cells. After Southern blot analysis screening, the successful ES clones were microinjected into blastocysts of C57BL/6J females. Finally, two independent ES clones generated germline chimeras. The chimeras were bred with C57BL6J mice to generate $CCKAR^{+/-}$ mutant F1 mice. $CCKAR^{-/-}$ mice were finally generated by mating $CCKAR^{+/-}$ mice followed by sufficient backcross to C57BL/6J wild-type mice. The experiments below were approved by the Committee of Animal Care of Kyusyu University and University of Toyama.

Locomotor activity recording

Wild-type and $CCKAR^{-/-}$ mice were housed in temperature-controlled (23±2°C) rooms, with a 12:12-h light-dark cycle. Food and water were provided *ad libitum*. To observe locomotor activity rhythms, mice were transferred to transparent plastic cages (30×35×17 cm), and their locomotor activity was measured using an infrared area sensor (F5B; Omron, Kyoto, Japan) located 30 cm above the surface of the cage. Locomotor activity was continuously recorded in 6-min epochs *via* a 48-channel parallel interface installed in a personal computer. To observe the free-running locomotor activity rhythm in constant darkness, wild-type (n=8) and $CCKAR^{-/-}$ (n=8) mice were housed in constant darkness for 2–3 wk. The free-running period during the first 2 wk was calculated using a χ^2 periodogram. For animals housed in constant darkness, circadian time 12 was defined as the onset of locomotor activities. To evaluate the response to photic stimuli, mice were maintained in constant darkness for 9 days and then exposed to a full-spectrum light pulse (15 min at 10–500 lux) at circadian time 16. The activity-onset delays in free-running rhythms were calculated on the basis of the distance between the two regression lines drawn from daily onset of locomotor activity for 7 days before and after the light pulse.

Pupillometry

Consensual pupillary constriction was measured in response to an adirectional light stimulus. Light was exposed for 60 s by a flexible-arm 100-W halogen lamp house (LA100USW; Hayashi Watch-Works Co. LTD., Tokyo, Japan), by which intensity was adjusted (20 or 100 lux at the animal levels) or maximized (>1000 lux). UV wavelength (<400 nm) was eliminated by a UV cut-filter installed in the lamp house. Adult male wild-type mice (n=5) and $CCKAR^{-/-}$ mice (n=4) were dark adapted for 1–2 h and placed on a custom-built stereotactic apparatus, by which animal movement was restricted by a 27 mmϕ polyethylene tube. Pupillary constriction was monitored with an infrared video system (BBCAM130 Night Vision-II; Timely Computer, Inc., Tokyo, Japan), which is composed of a digital charge-coupled device (CCD) camera centering on eight coaxial infrared (>850 nm) light-emitting diode arrays. At the end of the experiment, 1% atropine sulfate (Wako Pure Chemicals, Tokyo, Japan) dissolved in saline was dropped on the eye to estimate maximal pupil dimensions. Pupil dimensions were measured from the video images using Video Studio version 6.0 software (Ulead System, Inc., Tokyo, Japan). All experiments were conducted during the light period of 12:12-hour light-dark cycles.

5-Bromo-4-chloro-3-indoyl-β-D-galactopyranoside (X-gal) staining

Adult wild-type and $CCKAR^{+/-}$ mice (6 wk old) were used for the X-gal staining experiments. These animals were deeply anesthetized with an intraperitoneal injection of sodium pentobarbital (50 mg/kg body weight) and transcardially perfused with PBS for 5 min and then with ice-cold 2% paraformaldehyde in 0.1 M phosphate buffer for 15 min. Eyes

and the whole brain were removed and further fixed in the same fixative (4°C, 2 h). Then the vitreous and connective tissues were carefully removed from the eye, and the cerebellum and olfactory bulb were cut off from the brain in ice-cold PBS. The eyecups and brain tissue were immersed in 20% sucrose PBS and stored overnight. Frozen sections of 20 μm thickness were cut using a cryostat microtome and mounted on glass slides. These samples were then stained for 3 h at 37°C with a β-galactosidase (β-gal) staining kit (K1465–01; Invitrogen, Carlsbad, CA, USA) according to the manufacturer's instruction. As a negative control, samples from wild-type mice were also stained, but no staining was observed with a 3-h reaction period. These samples were imaged using a color CCD camera (Ds-5mc; Nikon, Tokyo, Japan) mounted on an inverted microscope (Axiovert 135TV with a Plan-Neofluar ×10 objective; Carl Zeiss, Thornwood, NY, USA).

Immunohistochemistry

Retinal frozen sections prepared as above were also used for immunofluorescence double-labeling studies. After three PBS rinses, the fixed samples were incubated in 10% donkey serum (Jackson ImmunoResearch Laboratories, West Grove, PA, USA) dissolved in 0.01% Triton X-100 (Sigma-Aldrich Corp., St. Louis, MO, USA) in PBS for 2 h at room temperature (22–26°C). As a first step, samples were incubated with 1:2000 mouse anti-β-galactosidase (Sigma-Aldrich Corp.) dissolved in 10% donkey serum in PBS for 24 h at 4°C. After three 20-min PBS rinses, samples were incubated in 1:200 Cy3-conjugated donkey anti-mouse IgG (Jackson ImmunoResearch Laboratories). As an additional staining step, 1:50 goat anti-Chx10 (Santa Cruz Biotechnology, Santa Cruz, CA, USA), 1:2000 goat anti-glycine transporter 1 (Chemicon International Inc., Temecula, CA, USA), 1:1000 goat anti-calretinin (Chemicon International Inc.), or 1:1000 rabbit anti-calbindin D28k (Chemicon International Inc.) was used as a primary antibody, and 1:200 fluorescein isothiocyanate (FITC) -conjugated donkey anti-goat IgG (Jackson ImmunoResearch Laboratories) or 1:200 FITC-conjugated donkey anti-rabbit IgG (Jackson ImmunoResearch Laboratories) was used as a secondary antibody. Double-labeled samples were embedded with Vectashield containing 4,6-diamidino-2-phenylindole (DAPI) (Vector Laboratories, Burlingame, CA, USA). The fluorescent images were acquired using a confocal laser-scanning unit (LSM510; Carl Zeiss) mounted on an inverted microscope (Axiovert 200M with an oil immersion objective lens, Plan-Apochromat ×63/1.40; Carl Zeiss).

Organotypic cultures

Wild-type and CCKAR$^{-/-}$ mouse pups (2–3 days old) were used to make organotypic cultures of retina and SCN. For retinal cultures, eyeballs were removed from the body after deep pentobarbital anesthesia and immediately immersed in ice-cold PBS. Under a stereomicroscope, the sclera and cornea were carefully torn and peeled off using fine forceps, and the neural retina was isolated. After removal of pigment epithelium and lens, the neural retina was trimmed using microscissors and placed in a 0.40-μm filter cup (Millicell-CM; Millipore, Bedford, MA, USA) with the ganglion cell layer being on the surface. The neural retinas on filter cups were transferred to standard six-well culture plates and cultured with 1 ml of low-glucose Dulbecco's modified Eagle's medium supplemented with 1:50 B-27 (Invitrogen), 5 μM forskolin (Sigma-Aldrich Corp.), 20 ng/ml brain-derived neurotrophic factor (Invitrogen), and 50 μg/ml gentamicin (Invitrogen). The medium was changed every other day until recording (7–14 days in culture). This procedure enables the survival of the outer and inner nuclear layers and the ganglion cell layer in the *in vitro* slice cultures (31).

SCN cultures were prepared as described previously (32). Briefly, coronal hypothalamic slices containing the SCN were cut using a vibrating-blade microtome in artificial cerebrospinal fluid containing 138.6 mM NaCl, 3.35 mM KCl, 21 mM $NaHCO_3$, 0.6 mM NaH_2PO_4, 9.9 mM D-glucose, 0.5 mM $CaCl_2$, and 3 mM $MgCl_2$ and bubbled with 95% O_2 and 5% CO_2. These slices were trimmed to an ~4-mm square containing the ventral end of the hypothalamus centered on the third ventricle. The slices were placed in Millicell-CM filter cups and cultured with 1 ml of medium consisting of 50% Eagle's basal medium, 25% Earle's balanced salt solution, and 25% heat-inactivated horse serum, supplemented with glucose and Glutamax (Invitrogen). The slice containing the rostrocaudal center of the SCN was used for further experiments. The SCN and retinal cultures were maintained in a CO_2 incubator at 35.5 ± 0.5°C and 5% CO_2.

Ca^{2+} imaging in retinal cultures

The retinal cultures on a membrane filter were incubated for 30 min in culture medium containing 10 μM Fura-2 AM (Molecular Probes, Eugene, OR, USA) in a CO_2 incubator at 35.5 ± 0.5°C and 5% CO_2 and rinsed 3× with buffered salt solution (BSS) consisting of 128 mM NaCl, 5 mM KCl, 2.7 mM $CaCl_2$, 1.2 mM $MgCl_2$, 1 mM Na_2HPO_4, 10 mM glucose, and 10 mM HEPES/NaOH (pH 7.3). Then the retinal cultures were gently removed from membrane filters using a fine brush and transferred to a recording chamber on the microscope. Fluorescent images were obtained with an upright microscope (Axioskop FS; Carl Zeiss) with a water immersion objective (Achroplan ×40 NA0.75; Carl Zeiss). The wavelength of the excitation UV light (340 or 380 nm pulse; 100 ms) was switched using a filter wheel (Lambda 10-2; Sutter Instruments, Novato, CA, USA). The UV light was generated by a full-spectrum 175-W xenon bulb (Lambda LS; Sutter) conducted to the microscope through a liquid light guide and reflected using a dichroic mirror (FT 395 nm; Carl Zeiss). The pair of fluorescent images were processed using a band-pass filter (BP 485–515 nm; Carl Zeiss) and exposed to a multiple-format cooled CCD camera (CoolSnap-FS; Photometrics, Tokyo, Japan) at 6-s intervals. The filter wheel and the CCD camera were controlled using digital imaging software (MetaFluor version 6.0; Japan Molecular Devices, Tokyo, Japan). The background fluorescence was also subtracted using the software. During recording, slices were placed in a 0.5-ml bath chamber and perfused with BSS supplemented with tetrodotoxin (0.5 μM) at a flow rate of 2.5 ml/min. CCK-8 sulfate (CCK-8s), lorglumide, thapsigargin (all purchased from Sigma-Aldrich Corp.), Ca^{2+}-free BSS, and 60 mM potassium (high K^+) BSS were applied by switching the perfusate.

Ca^{2+} imaging in SCN cultures

Isolation of neuronal and glial images is difficult in SCN slices using conventional Fura-2 AM staining methods; therefore, neuron-specific Ca^{2+} imaging was performed using a yellow cameleon 2.1 sensor linked to a neuron-specific enolase promoter (32). The cameleon-expressing SCN slice was cut from a filter cup and transferred into the microscope chamber together with the membrane filter. The Ca^{2+} response was observed as above using an upright microscope with an ×40 water-immersion objective. The SCN neurons were exposed to 440 ± 5 nm light using a liquid light guide lamp house (Lambda LS) with a band-pass filter (440NBD10; Omega Optical Inc., Brattleboro, VT, USA). The resultant fluorescence image was separated using a dichroic mirror (455DRLP; Omega Optical Inc.) and fed into double-view

optics (A4313; Hamamatsu Corporation, Bridgewater, NJ, USA), in which one image was split into bilateral images *via* internal reflection mirrors and processed using two dichroic mirrors (515 DRLPXR; Omega Optical Inc,) and band-pass filters (480DF30 and 535DF25 filters). The lamp house, shutter, and CCD camera were controlled as above using digital imaging software.

Quantitative reverse transcriptase-polymerase chain reaction (PCR)

Total RNA was extracted from mouse tissue using RNAzolB reagent (Tel-Test Inc., Friendswood, TX, USA). Mice were deeply anesthetized with ether, and their brains were quickly removed. Coronal brain slices (1 mm) were prepared using a rodent brain matrix (RBM-2000C; ASI Instruments, Warren, MI, USA), and the SCN was punched out bilaterally from the brain slices. The cDNAs of *mPer1* (GenBank accession number AF022992; sense, 5′-CCAGGCCCGGAGAACCTTTTT-3′; antisense, 5′-CGAAGTTTGAGCTCCCGAAGTG-3′), *mPer2* (GenBank accession number AF035830; sense, 5′-ACACCACCCCTTACAAGCTTC-3′; antisense, 5′-CGCTGGATGATGTCTGGCTC-3′), CCK-A receptor (GenBank accession number AK004730; sense, 5′-ACAGGAGTGAGCCATTCACCAGC-3′; antisense, 5′-GATGTTGGTGACAGTCCGCATCC-3′), and mouse glyceraldehyde-3-phosphate dehydrogenase (GAPDH) (GenBank accession number M32599; sense, 5′-GGGAAGCTTGTCATCAA-3′; antisense, 5′-TGCTTCA-CCACCTTCTTG-3′) were amplified using a program temperature control system PC-700 (ASTEC, Fukuoka, Japan). The reaction solution consisted of 2.5 μl of 10× PCR buffer (Boehringer Mannheim, Mannheim, Germany), 2.5 μl of 2.5 mM dNTP, 1.25 μl of 10 μM sense, 1.25 μl of 10 μM antisense, 17.0 μl of distilled water, 0.25 μl of *Taq* polymerase (Boehringer Mannheim), and 0.2 μl of 20 μCi [^{32}P]dCTP (Amersham Pharmacia Biotech, Ltd., Little Chalfont, Buckinghamshire, UK). The PCR product was run on a 5% acrylamide gel. Images were visualized using an imaging plate (BAS-IP MS 2040; Fujifilm, Tokyo, Japan) and analyzed using Image Gauge (Fujifilm). The exponential phase of GAPDH amplification in all experimental conditions was located between cycles 22 and 24, and the exponential phase of *mPer1* and *mPer2* was located between cycles 29 and 31. The amplified efficiency of GAPDH and *mPer1* or *mPer2* was quantified at cycle 30. The ratio of the amplified target to the amplified internal control was compared.

In situ hybridization

Mice were deeply anesthetized with ether and intracardially perfused with chilled saline (25 ml) followed by 0.1 M phosphate buffer (pH=7.4) containing 4% paraformaldehyde (25 ml). Brains were removed, postfixed in 0.1 M phosphate buffer containing 4% paraformaldehyde for 24 h at 4°C, and transferred into 20% sucrose in 0.1 M phosphate buffer for 72 h at 4°C. Slices (40 μm thick) that included the SCN were cut using a cryostat and divided into three equal groups from rostral to caudal regions for the measurement of *mPer1* and *mPer2* mRNAs. The *mPer1* and *mPer2* cRNA probes were a gift from Dr. Hitoshi Okamura at Kobe University (nucleotide positions: *mPer1*, 538–1752; *mPer2*, 1–638) for use in these *in situ* hybridization studies. Slices were placed in 2× standard sodium citrate (SSC) and were treated with 1 μg/ml proteinase K in 10 mM Tris-HCl buffer (pH=7.5) containing 10 mM EDTA for 10 min at 37°C, followed by treatment with 0.25% acetic anhydride in 0.1 M triethanolamine and 0.9% NaCl for 10 min. The slices were then incubated in hybridization buffer [60% formamide, 10% dextran sulfate, 10 mM Tris-HCl (pH=7.4), 1 mM EDTA, 0.6 M NaCl, Denhardt's solution (0.02% Ficoll, 0.02% polyvinyl pyrrolidone, and 0.02% bovine serum albumin), 0.2 mg/ml tRNA, and 0.25% sodium dodecyl sulfate] containing ^{33}P-labeled cRNA probes for 16 h at 60°C. Radioisotope (α[α-^{33}P]UTP; PerkinElmer Life and Analytical Sciences, Boston, MA, USA) -labeled antisense cRNA probes were made from restriction enzyme-linearized cDNA templates. After high-stringency posthybridization washes with 2× SSC/50% formamide, slices were treated with RNaseA (10 μg/ml) for 30 min at 37°C. Images were prepared as autoradiograms using BioMax MR film (Eastman Kodak, Rochester, NY, USA). After conversion into optical density by ^{14}C-autoradiographic microscales (Amersham Biosciences Corp., Piscataway, NJ, USA), they were analyzed using an image analysis system (MCID; Imaging Research, St. Catharines, ON, Canada). Further, mounted slices after exposure to X-ray film were dipped into emulsion (NTB2, diluted 1:1 with distilled water; Eastman-Kodak), air-dried for 3 h, and stored in light-tight slide boxes at 4°C for 3 wk. The slides were developed with a D19 developer (Eastman Kodak), fixed with Fujifix (Fujifilm), and counterstained with cresyl violet (Sigma-Aldrich Corp.).

Statistical analysis

All data are presented as means with SE. Unless otherwise noted, one-way ANOVA followed by Duncan's multiple-range tests was used for the statistical comparisons across multiple means. Two-tailed Student's *t* test was used for the pairwise comparisons. A 95% confidence level was considered to indicate statistical significance. The irradiance dependency for the pupillary light reflex was analyzed using two-way ANOVA. The irradiance response curve for circadian phase shifts was analyzed using a four-parameter Hill function using SigmaPlot software (version 7.1; SPSS Inc., Chicago, IL, USA).

RESULTS

Robust expression of CCK-A receptors in glycinergic amacrine cells in the photic input pathways to the circadian clock

To visualize CCK-A receptors in the photic input pathways to the SCN clock, we examined X-gal staining using serial sections of retina and brain of heterozygous mutant (CCKAR$^{+/-}$) mice. In the retina, staining was robust throughout the inner nuclear layer (**Fig. 1*A***). Within the SCN, only scattered staining was observed in the core region, whereas the shell boundary zone (peri-SCN) and periventricular zone contained a relatively larger number of stained cells (Fig. 1*B*). The number of stained cells in the SCN was less than that in control hypothalamic regions, such as in the arcuate nuclei (number of X-gal stained cells=23.8±6.6/SCN slice and 137.6±19.4/rostral arcuate nucleus slice, number of slices=5, $P<0.01$ by Student's *t* test; Fig. 1*C*).

To determine the cell types in the retina that express CCK-A receptors, we examined double immunofluorescent staining of retina with antibodies against β-gal and several different neural markers (**Fig. 2**). Staining with the amacrine cell marker, glycine transporter-1, was strongly colocalized with β-gal staining (74.6±3.5%, number of slices=5). Neither calretinin-positive amacrine cells nor calbindin-D28k-positive amacrine cells exhibited β-gal staining (number of slices=5). Also, neither horizontal cells visualized using calbindin-D28k

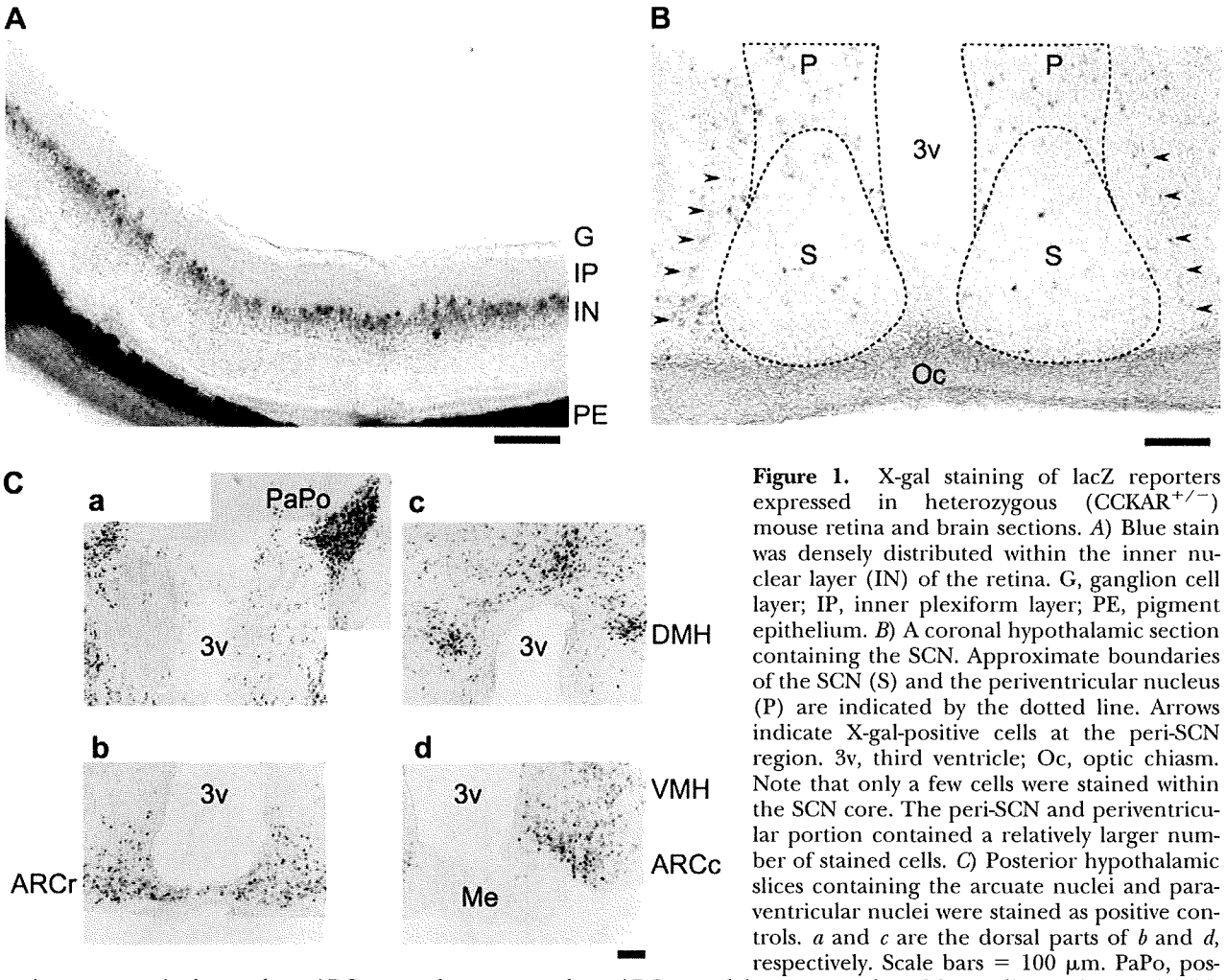

Figure 1. X-gal staining of lacZ reporters expressed in heterozygous ($CCKAR^{+/-}$) mouse retina and brain sections. *A*) Blue stain was densely distributed within the inner nuclear layer (IN) of the retina. G, ganglion cell layer; IP, inner plexiform layer; PE, pigment epithelium. *B*) A coronal hypothalamic section containing the SCN. Approximate boundaries of the SCN (S) and the periventricular nucleus (P) are indicated by the dotted line. Arrows indicate X-gal-positive cells at the peri-SCN region. 3v, third ventricle; Oc, optic chiasm. Note that only a few cells were stained within the SCN core. The peri-SCN and periventricular portion contained a relatively larger number of stained cells. *C*) Posterior hypothalamic slices containing the arcuate nuclei and paraventricular nuclei were stained as positive controls. *a* and *c* are the dorsal parts of *b* and *d*, respectively. Scale bars = 100 μm. PaPo, posterior paraventricular nucleus; ARCr, rostral arcuate nucleus; ARCc, caudal arcuate nucleus; Me, median eminence; DMH, dorsal medial hypothalamus; VMH, ventral medial hypothalamus.

staining nor bipolar cells visualized using Chx10 staining exhibited β-gal staining (number of slices=5). These results clearly indicate that CCK-A receptors were expressed specifically on amacrine cells, most of which also expressed glycine transporters.

Stimulation of CCK-A receptors mobilized intracellular Ca^{2+} in retinal amacrine cells but not in SCN neurons

We used Ca^{2+} imaging of organotypic cultures of retina and SCN to analyze the functional expression of CCK-A receptors within the photic input pathways to the circadian clock. First, Fura-2 AM-stained retinal cultures of wild-type (n=8), $CCKAR^{+/-}$ (n=8), and $CCKAR^{-/-}$ (n=8) mice were stimulated using the CCK-A receptor agonist, CCK-8s (300 nM, 1 min). CCK-8s evoked Ca^{2+} transients in 7.1 ± 1.8% of the Fura-2 AM-stained cells (total number of cells=234) in wild-type retina and 5.7 ± 1.9% of the cells (total number of cells=228) in $CCKAR^{+/-}$ retina (**Fig. 3*A*, *C***). These responding cells were identified as amacrine cells by the postexperimental X-gal staining of $CCKAR^{+/-}$ retina (Fig. 3*C*). The CCK-8s-induced Ca^{2+} transient but not the high K^+-induced Ca^{2+} flux was absent in $CCKAR^{-/-}$ retina (total number of cells=230) (Fig. 3*A*, *C*). The CCK-8s-induced Ca^{2+} transient observed in wild-type retina was significantly inhibited using the CCK-A antagonist, lorglumide (300 nM, application 5 min before the CCK-8s application; $F_{5,42}$=7.08, P<0.01 by one-way ANOVA followed by Duncan's multiple-range tests) (Fig. 3*C*). The CCK-8s-induced Ca^{2+} transients observed in wild-type retinas were resistant to the replacement of normal extracellular buffer with Ca^{2+}-free buffer (responding cell population=7.8±2.2%, total number of cells=215). CCK-8s-induced Ca^{2+} transients were completely eliminated, however, after thapsigargin-depletion of internal Ca^{2+} stores ($F_{5,42}$=7.08, P<0.01 by one-way ANOVA followed by Duncan's multiple-range tests) (Fig. 3*B*, *C*).

Second, organotypic slice cultures of SCN expressing a yellow cameleon 2.1 sensor linked to a neuron-specific enolase promoter were used to examine the effects of exposure to either CCK-8s or glutamate (**Fig. 4**). Within the core region, ~75% of cultured SCN neurons (55 of 73 neurons, number of slices=11) exhibited a significant increase in cytosolic Ca^{2+} in response to exposure to glutamate (300 μM, 1 min), but exhibited no response to CCK-8s (300 nM, 1 min) (Fig. 4*A*). A similar response to

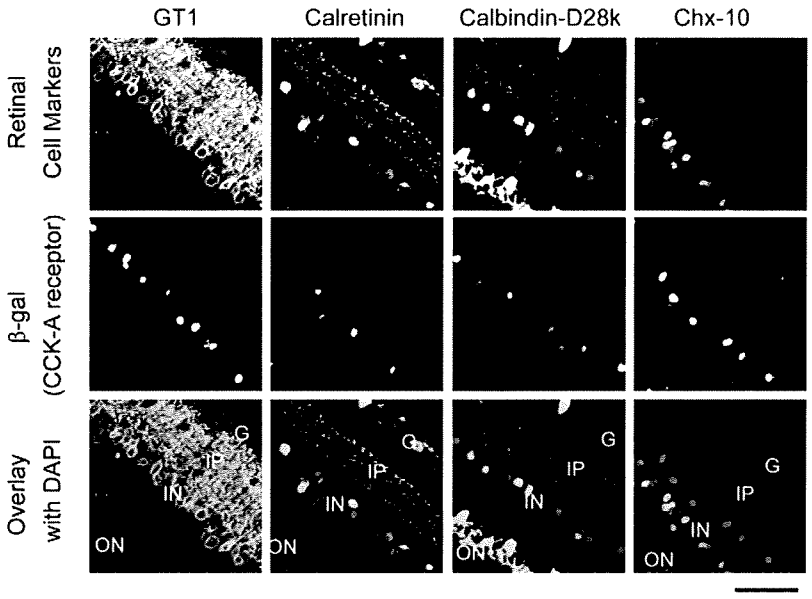

Figure 2. Immunofluorescent staining of heterozygous (CCKAR$^{+/-}$) mouse retina. The lacZ reporters stained with anti-β-gal antibody (middle row, shown as red in the bottom row), immunostaining for several retinal cell markers (top row, indicated above, shown as green in the bottom row), and counterstaining with DAPI (blue in the bottom row) were viewed and superimposed using a confocal scanning microscope. Anti-glycine transporter 1 (GT1) stains the plasma membrane of cell bodies and dendrites of glycinergic amacrine cells specifically. β-Gal staining strongly colocalized with GT1 staining of cell bodies (asterisks on the overlay image). Anti-calretinin antibody and/or anti-calbindin-D28k antibody recognizes another class of amacrine cells, horizontal cells, and/or ganglion cells, all of which did not colocalize with β-gal staining. Also, bipolar cells stained with anti-Chx10 antibody were not colocalized with β-gal stain. Scale bar = 50 μm. ON, outer nuclear layer; IN, inner nuclear layer; IP, inner plexiform layer; G, ganglion cell layer.

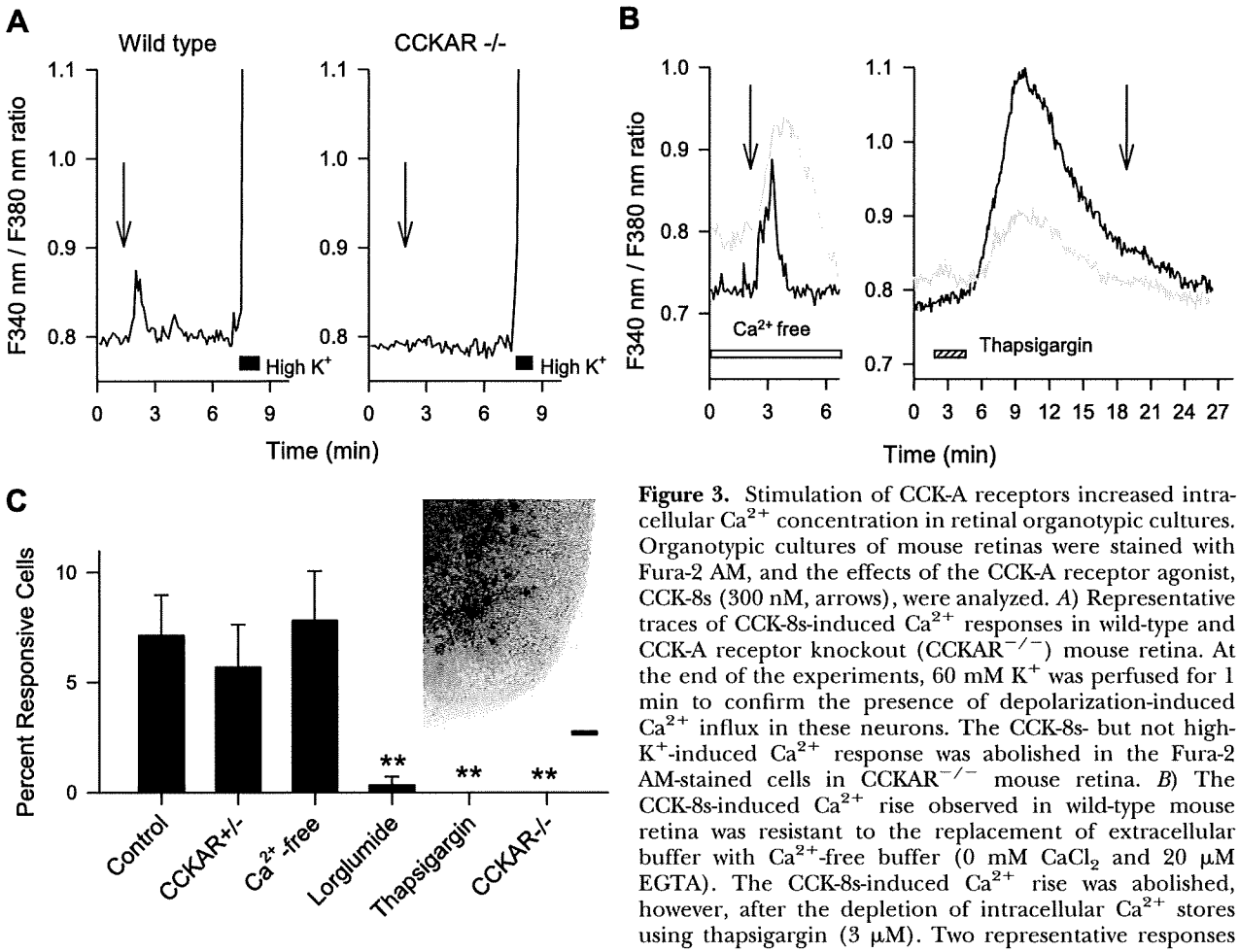

Figure 3. Stimulation of CCK-A receptors increased intracellular Ca^{2+} concentration in retinal organotypic cultures. Organotypic cultures of mouse retinas were stained with Fura-2 AM, and the effects of the CCK-A receptor agonist, CCK-8s (300 nM, arrows), were analyzed. *A*) Representative traces of CCK-8s-induced Ca^{2+} responses in wild-type and CCK-A receptor knockout (CCKAR$^{-/-}$) mouse retina. At the end of the experiments, 60 mM K^+ was perfused for 1 min to confirm the presence of depolarization-induced Ca^{2+} influx in these neurons. The CCK-8s- but not high-K^+-induced Ca^{2+} response was abolished in the Fura-2 AM-stained cells in CCKAR$^{-/-}$ mouse retina. *B*) The CCK-8s-induced Ca^{2+} rise observed in wild-type mouse retina was resistant to the replacement of extracellular buffer with Ca^{2+}-free buffer (0 mM $CaCl_2$ and 20 μM EGTA). The CCK-8s-induced Ca^{2+} rise was abolished, however, after the depletion of intracellular Ca^{2+} stores using thapsigargin (3 μM). Two representative responses from different cells (black and gray) are shown. *C*) Percentage of the retinal cells responding to CCK-8s. The CCK-A receptor antagonist, lorglumide (300 nM), also inhibited the CCK-8s-induced Ca^{2+} response. $^{**}P < 0.01$ by one-way ANOVA followed by Duncan's multiple-range tests. Inset: The CCK-8s-induced Ca^{2+} response was exclusively observed in amacrine cells, which were postexperimentally identified by X-gal (blue) staining in organotypic cultures of CCKAR$^{+/-}$ mouse retina. Scale bar = 100 μm.

glutamate was observed in slice cultures of CCKAR$^{-/-}$ mouse SCN (14 of 20 neurons, number of slices=3). Of a total of 73 neurons analyzed in the wild-type slice, one neuron in the dorsomedial periventricular region exhibited a sustained increase in cytosolic Ca^{2+} in response to CCK-8s, and this effect was completely inhibited in the presence of lorglumide (300 nM) (Fig. 4*B*). The amplitude of the glutamate response after exposure to CCK-8s was similar to that in the presence of lorglumide in this particular neuron.

Light pulse-induced *mPer1* and *mPer2* gene expression was reduced in the SCN of CCKAR$^{-/-}$ mice

To examine the effects of CCKAR$^{-/-}$ on light-induced responses of SCN neurons, we examined quantitative PCR for *mPer1* and *mPer2* mRNAs in SCN grafts. Under constant darkness conditions, the levels of *mPer1* and *mPer2* mRNAs oscillated in a circadian fashion both in the wild-type and CCKAR$^{-/-}$ SCN (**Fig. 5*A*, *B***). The approximate peaks of *mPer1* and *mPer2* occurred at identical times in the wild-type and CCKAR$^{-/-}$ SCN: at circadian time 6 for *mPer1* and at circadian time 9 for *mPer2* (Fig. 5*B*). Brief light pulse exposure (70 lux, 15 min) applied 4 h after the activity-onset time (circadian time 16), significantly increased the expression of *mPer1* (3.2-fold of unexposed control; $P<0.01$ by Student's *t* test) and *mPer2* (3.6-fold of unexposed control; $P<0.01$ by Student's *t* test) in the wild-type SCN (Fig. 5*C*). The light pulse-induced *mPer1* expression (1.6-fold of unexposed control; $P=0.16$ by Student's *t* test) and *mPer2* expression (1.7-fold of unexposed control; $P=0.09$ by Student's *t* test) were less evident in the SCN grafts of CCKAR$^{-/-}$ mice (Fig. 5*C*). The light pulse-induced increase in *mPer1* and *mPer2* mRNAs in wild-type SCN and the reduction in the responsiveness in the CCKAR$^{-/-}$ SCN were also visualized using *in situ* hybridization in SCN sections (Fig. 5*D*).

Light pulse-induced behavioral phase shifts and pupillary reflex were reduced in CCKAR$^{-/-}$ mice

Infrared sensor detection of activity/rest patterns across 24-h light-dark cycles (data not shown) and free-running periods of behavioral rhythms in constant darkness (**Fig. 6*A***) were almost identical between wild-type mice ($\tau=23.8\pm0.06$ h, $n=8$) and CCKAR$^{-/-}$ mice ($\tau=23.9\pm0.04$ h, $n=8$). The magnitude of behavioral phase delays caused by a light pulse exposure (10–500 lux for 15 min) at circadian time 16 was analyzed in wild-type and CCKAR$^{-/-}$ mice. Both types exhibited activity-onset delays depending on the intensity of light exposure (Fig. 6*B*). The magnitude of the phase delays caused by 50 lux or larger, however, was significantly smaller in CCKAR$^{-/-}$ mice than in wild-type mice. The maximal reduction in responsiveness was observed at 50 lux, at which CCKAR$^{-/-}$ mice exhibited a 42% smaller magnitude in phase shift than that of wild-type mice ($P<0.05$ by Student's *t* test, $n=8$ for both types). The maximal response at 500 lux was still 35% smaller in CCKAR$^{-/-}$ mice ($P<0.01$ by Student's *t* test, $n=8$ for both types) (Fig. 6*B*).

To examine the effects of CCKAR$^{-/-}$ on nonimage-forming visual functions, we further analyzed the consensual pupillary reflex using infrared video systems. The dark-adapted aperture areas were not significantly different between the wild-type mice (2.43 ± 0.07 mmϕ, $n=5$) and CCKAR$^{-/-}$ mice (2.48 ± 0.03 mmϕ, $n=4$). Also, atropine-induced aperture areas observed at the end

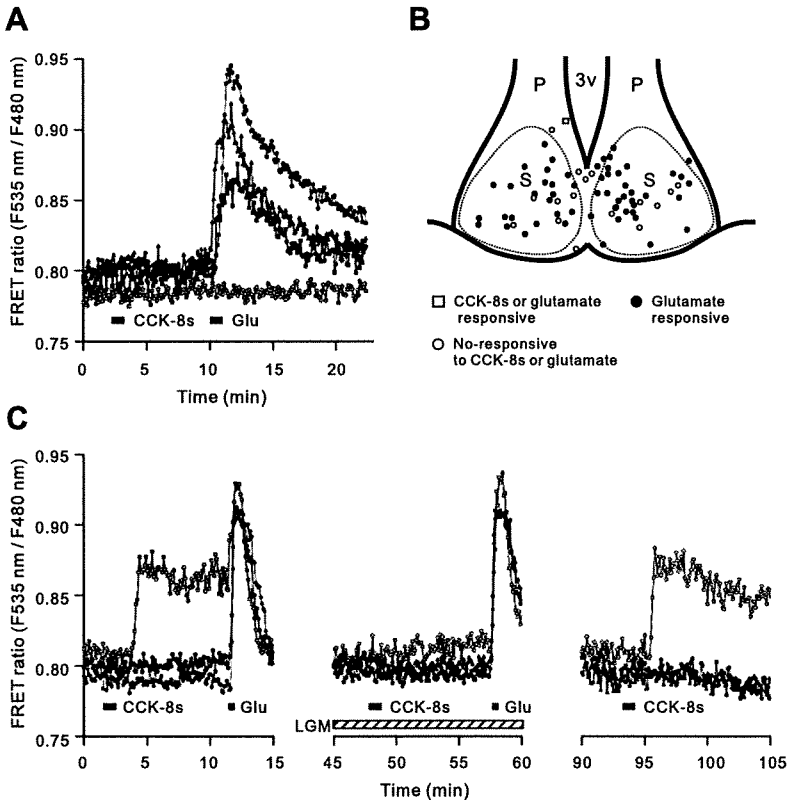

Figure 4. CCK-A receptors were not expressed in retino-recipient SCN neurons. Yellow cameleon 2.1 imaging of organotypic SCN cultures was used to investigate CCK-A receptor function in SCN neurons. A total of 73 neurons in wild-type SCN were exposed to CCK-8s (300 nM) followed by glutamate (Glu) (300 μM). *A*) Example cytosolic Ca^{2+} levels in four neurons. The cytosolic Ca^{2+} concentration increased in response to exposure to glutamate in three of four neurons shown. *B*) Approximate distribution of recorded neurons in the SCN (S) and the periventricular nucleus (P). Glutamate-induced Ca^{2+} responses were observed in neurons distributed throughout the SCN. CCK-8s did not mobilized cytosolic Ca^{2+} in 72 cells. 3v, third ventricle. *C*) One exception was found in the dorsomedial periventricular area (shown as a gray square in *B*), in which the cytosolic Ca^{2+} concentration increased in response to either CCK-8s or glutamate. The Ca^{2+} response to CCK-8s was inhibited by lorglumide (LGM) (300 nM).

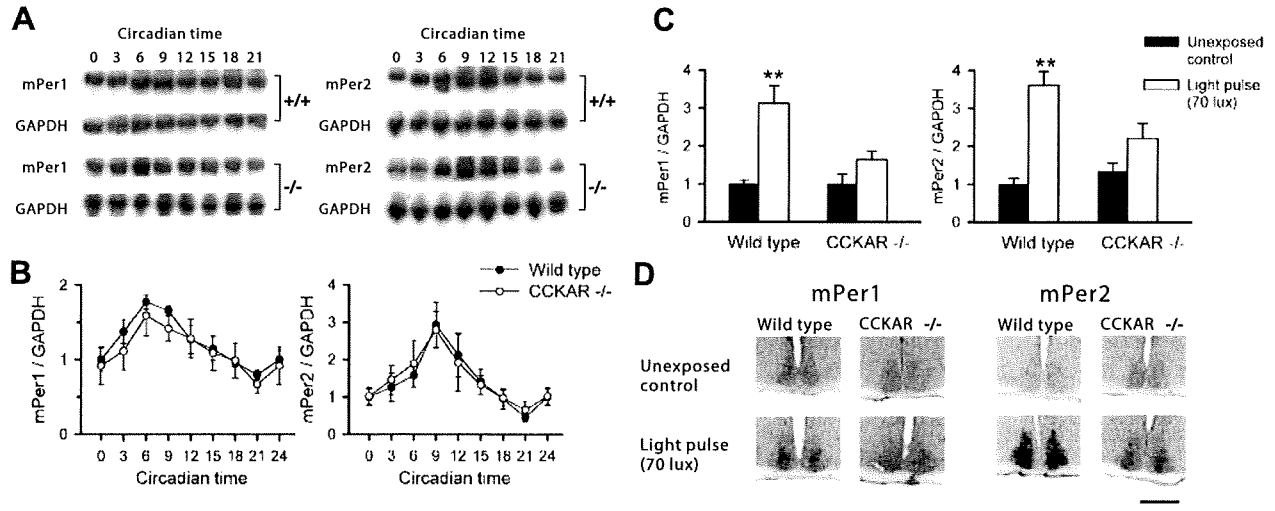

Figure 5. Light pulse-induced *mPer1* and *mPer2* gene expression was reduced in CCKAR$^{-/-}$ mice. *A*) Example blotting of *mPer1* and *mPer2* using wild-type SCN (+/+) and CCK-A receptor knockout SCN (−/−), both of which were sampled from mice maintained in constant darkness. *B*) *mPer1* and *mPer2* mRNA levels were quantified in terms of GAPDH mRNA levels. Circadian rhythms in *mPer1* and *mPer2* mRNA levels were observed in the SCN regardless of the genotypes. *C*) A light pulse (15 min, 70 lux) at circadian time 16 elevated *mPer1* and *mPer2* mRNA levels in the wild-type SCN sampled 60 min later. $^{**}P < 0.01$ by Student's *t* test. The light pulse-induced *mPer1* and *mPer2* mRNA expression was less evident in CCKAR$^{-/-}$ mice. $n = 4$ for each group. *D*) Topographical analysis of *mPer1* and *mPer2* mRNA expression in the SCN was also examined using *in situ* hybridization. The light pulse was applied as above to estimate the light-induced *mPer1* and *mPer2* mRNA expression in the SCN. Scale bar = 500 μm.

of experiments were not significantly different between the wild-type mice (2.60±0.08 mmϕ, n=5) and CCKAR$^{-/-}$ mice (2.67±0.09 mmϕ, n=4). The irradiance-dependent pupillary constrictions caused by 20, 100, or >1000 lux light were also observed both for the wild-type mice ($F_{2,92}$=440.2, P<0.01 by two-way ANOVA) and CCKAR$^{-/-}$ mice ($F_{2,92}$=183.9, P<0.01 by two-way ANOVA for the wild-type group) (**Fig. 7*A***). However, the minimal pupillary dimensions followed by exposures of 100-lux light (+64.7%; P<0.05 by Student's *t* test) or >1000-lux light (+154.3%; P<0.05 by Student's *t* test) were significantly larger in CCKAR$^{-/-}$ mice (Fig. 7*B, C*).

DISCUSSION

The results of the present study demonstrate that in mice there is robust expression of CCK-A receptors on retinal glycinergic amacrine cells, with relatively little expression on SCN neurons that receive projections from the retina. Also, a CCK-A agonist induced intracellular Ca^{2+} mobilization in amacrine cells and not SCN neurons. Moreover, mutant mice deficient in CCK-A receptors exhibited reduced light pulse-induced *mPer1/mPer2* gene expression in the SCN. Furthermore, light pulse-induced behavioral phase shifts and pupillary reflex were also significantly reduced in CCKAR$^{-/-}$ mice. Taken together, these data indicate that functional CCK-A receptors located primarily on amacrine cells are the most significant cause for circadian modulation of *mPer1/mPer2* gene expression in the SCN and can modulate nonimage-forming visual functions. Thus, we suggest a novel function of CCK-A receptors in retinal signal processing.

Little CCK function in retino-recipient SCN neurons

CCK peptides have previously been reported to be expressed to some degree in SCN neurons (6, 15–17), so we carefully analyzed the possible functionality of CCK-A receptors in SCN neurons. X-gal stained only sparsely scattered cells in the SCN, with a rather denser distribution in the peri-SCN and periventricular zones. Consistent with this result, our Ca^{2+} imaging studies in organotypic SCN cultures demonstrated that core SCN neurons did not respond to the CCK-A receptor agonist, CCK-8s. An increase in cytosolic Ca^{2+} evoked by either CCK-8s or glutamate was observed in only one neuron located in the periventricular region, where retino-recipient neurons are absent or rare (16). Although lack of CCK-8s effects on glutamate receptive SCN neurons may be due to limitations of samples in our Ca^{2+} imaging studies, this result is consistent with the reported distribution of CCK peptides in the mouse, because dorsal efferent fibers from the SCN but not retinohypothalamic tracts are CCK-immunoreactive in mice (16). Therefore, CCK peptides may have a role in the efferent transmission from SCN neurons and/or transmission between intra-SCN neurons but not for transmission to retino-recipient SCN neurons.

Because CCK is one of the most abundant neuropeptides in the brain, and several brain loci responsible for visual input, such as the dorsal lateral geniculate, express CCK-A receptors (33), careful discussion is needed to identify the localization of CCK-A receptors responsible for the modulation of nonimage-forming visual functions. The SCN receive geniculohypothalamic tracts (GHT) from the intergeniculate leaflet (IGL) of the thalamus (6). It has been shown that the GHT uses neuropeptide-Y and GABA as neurotransmitters to the SCN, and this pathway is involved in the

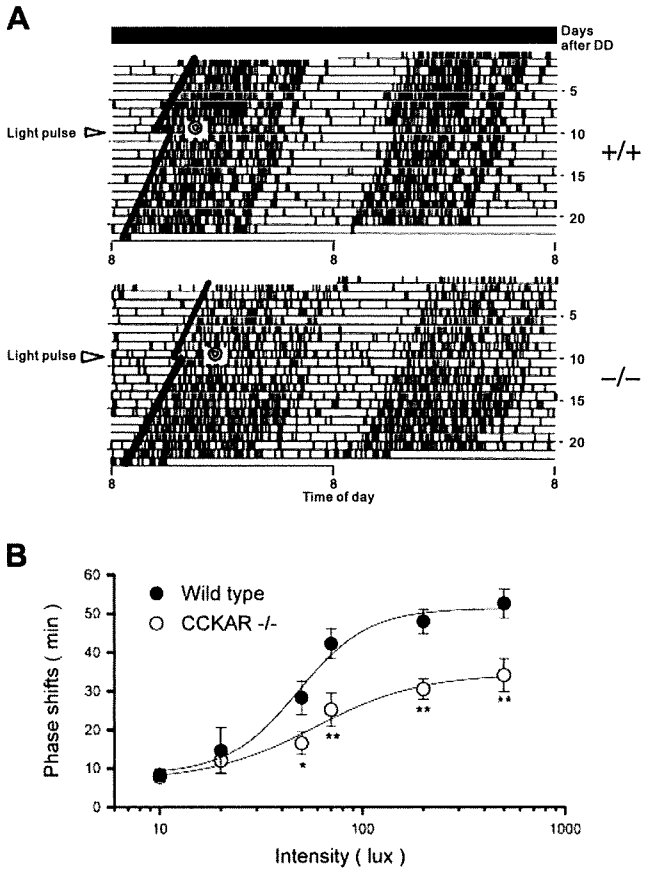

Figure 6. Light pulse-induced behavioral phase shifts were reduced in CCKAR$^{-/-}$ mice. *A*) Representative double-plot actograms showing circadian phase delays in response to a light pulse (15 min, 50 lux) in a wild-type mouse (+/+) and a CCKAR$^{-/-}$ mouse (−/−). Double circles denote the timing of the light pulse exposure at circadian time 16. The approximate activity-onset time is indicated on the left-hand actograms (lines fitted by eye). *B*) Irradiation response curve for the circadian phase shifts evoked by a 15-min light pulse applied at circadian time 16. Although both genotypes exhibited an intensity-dependent increase in the magnitude of the phase shifts, CCKAR$^{-/-}$ mice exhibited shorter circadian phase delays when the light pulse was more intense than 50 lux. n = 4–11 in each group. $^{*}P < 0.05$ and $^{**}P < 0.01$ in comparison with the corresponding wild-type group by Student's t test.

behavioral phase shifts *via* nonphotic inputs, such as that *via* activity elevations and triazolam administrations (6). Also, it has been shown that a free running period during constant light is reduced by IGL lesions, and thus the GHT pathway may be involved in the tonic effects of light (6). However, to our knowledge, there have been no reports showing that light pulse-induced phase shifts are significantly modulated by IGL lesions in mice. Whether CCK-A receptors are expressed on any of the GHT pathways to the SCN is currently not known; therefore, it is reasonable to consider that significant reduction of photoentrainment in CCKAR$^{-/-}$ mice is due to the modulation of reticulohypothalamic (RHT) pathways not of GHT pathways. Within the RHT pathways, the results of the lacZ reporter assays and Ca^{2+} imaging in the present study suggest that the principal site of CCK-A receptor actions for circadian photoentrainment is confined within the retina not in SCN neurons.

Possible function of CCK-A receptors in mouse amacrine cells

Approximately 30 different types of amacrine cells have been identified in the mammalian retina (34). About half of the amacrine cells contain GABA and the other half contain glycine as inhibitory neurotransmitters, and both of these types of amacrine cells express ionotropic glutamate receptors to receive glutamatergic input from bipolar cells (35). Despite the abundant knowledge about the morphological diversity of amacrine cells, their physiological functions are poorly understood, especially at a systems level. One of the best characterized functions is inhibitory neurotransmission on the synapse between bipolar cells and retinal ganglion cells (36). This amacrine cell function contributes to the transient firing pattern of retinal ganglion cells, which is required for background control for motion perception (37, 38). The present results suggest that amacrine cells have a novel role in circadian photoentrainment, because *1*) CCK-A receptors were concentrated on glycine transporter-positive amacrine cells but not on retino-recipient SCN neurons, *2*) a CCK-A receptor agonist evoked calcium responses in amacrine cells of wild-type but not of CCKAR$^{-/-}$ mice nor in the SCN of wild-type mice, *3*) CCKAR$^{-/-}$ mice exhibited reduced light pulse-induced *mPer1/mPer2* expression in the SCN, and *4*) CCKAR$^{-/-}$ mice exhibited reduced light pulse-induced behavioral phase shifts. Notably, these results suggest that CCK-A receptor activation results in an excitatory effect on retinal ganglion cells that project to the SCN, because the photic response of the SCN was significantly reduced in CCKAR$^{-/-}$ mice.

The present results showed that the cytosolic Ca^{2+} concentration was increased by CCK-8s in cultured amacrine cells. Activation of phospholipase C with generation of inositol 1,4,5-trisphosphate and diacylglycerol, subsequent Ca^{2+} release from internal Ca^{2+} stores, and activation of protein kinase C is the proposed intracellular signaling common to a wide variety of cells after CCK-A receptor activation (39–41). Accordingly, the CCK-8s-induced Ca^{2+} response in cultured amacrine cells remained in Ca^{2+}-free extracellular medium but was abolished by the depletion of internal Ca^{2+} stores by thapsigargin. In chick retinal cultures, protein kinase Cγ colocalizes with α-amino-3-hydroxy-5-methyl-4-isoxazole-propionic acid (AMPA) -type glutamate receptors, and phosphorylation of AMPA receptors by protein kinase C causes translocation of AMPA receptors to the plasma membrane and increases excitatory synaptic transmission (42). Axons from glycinergic amacrine cells have been reported to terminate on neighboring GABAergic amacrine cells, which terminate on the synapse between bipolar cells and retinal ganglion cells (38). Therefore, one possible explanation of the excitatory action of CCK-A receptor activation on the ON bipolar-ganglion cell synapse is that activation of CCK-A receptors excites glycinergic amacrine cells, which inhibit GABAergic amacrine